The evolutionarily conserved choroid plexus contributes to the homeostasis of brain ventricles in zebrafish

Inyoung Jeong, Søren N Andreassen, Linh Hoang, Morgane Poulain, Yongbo Seo, Hae-Chul Park, Maximilian Fürthauer, Nanna Macaulay, Nathalie Jurisch-Yaksi

Cell Reports

The evolutionarily conserved choroid plexus contributes to the homeostasis of brain ventricles in zebrafish

Graphical abstract

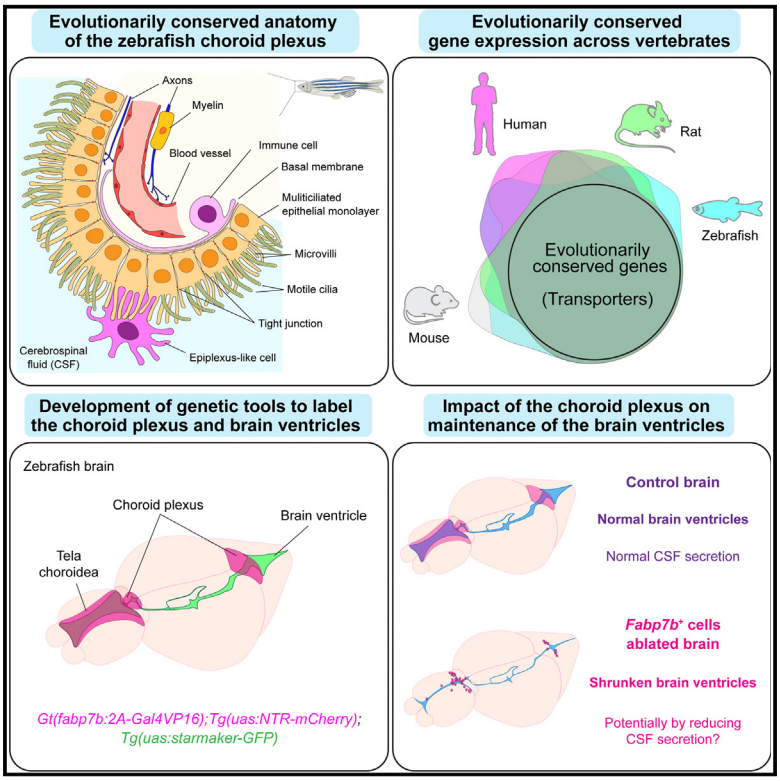

Highlights

- The zebrafish and mammalian choroid plexus have similar anatomical features
- The expression of transporters involved in CSF secretion is evolutionarily conserved
- The choroid plexus epithelial cells express *fabp7* and secrete proteins into CSF
- Ablation of *fabp7b*-expressing cells decreases the size of the brain ventricles

Authors

Inyoung Jeong, Søren N. Andreassen, Linh Hoang, ..., Maximilian Fürthauer, Nanna MacAulay, Nathalie Jurisch-Yaksi

Correspondence

nathalie.jurisch-yaksi@ntnu.no

In brief

Jeong et al. show that the zebrafish choroid plexus has conserved anatomical features with mammals and expresses transporters involved in cerebrospinal fluid secretion. By using chemogenetics, they reveal that ablation of choroid plexus epithelial cells decreases the size of the brain ventricles.

Jeong et al., 2024, Cell Reports *43*, 114331
June 25, 2024
https://doi.org/10.1016/j.celrep.2024.114331

CellPress

Cell Reports

CellPress
OPEN ACCESS

Report

The evolutionarily conserved choroid plexus contributes to the homeostasis of brain ventricles in zebrafish

Inyoung Jeong,[1] Søren N. Andreassen,[2] Linh Hoang,[3] Morgane Poulain,[4] Yongbo Seo,[5] Hae-Chul Park,[5] Maximilian Fürthauer,[4] Nanna MacAulay,[2] and Nathalie Jurisch-Yaksi[1,6,*]

[1]Department of Clinical and Molecular Medicine, Norwegian University of Science and Technology, Erling Skjalgsons Gate 1, 7491 Trondheim, Norway

[2]Department of Neuroscience, University of Copenhagen, Blegdamsvej 3, 2200 Copenhagen, Denmark

[3]Cellular and Molecular Imaging Core Facility (CMIC), Norwegian University of Science and Technology, Erling Skjalgsons Gate 1, 7491 Trondheim, Norway

[4]Université Côte d'Azur, CNRS, Inserm, iBV, 28 Avenue Valrose, 06108 Nice cedex 2, France

[5]Department of Biomedical Sciences, Korea University College of Medicine, Seoul 02841, Republic of Korea

[6]Lead contact

*Correspondence: nathalie.jurisch-yaksi@ntnu.no

https://doi.org/10.1016/j.celrep.2024.114331

SUMMARY

The choroid plexus (ChP) produces cerebrospinal fluid (CSF). It also contributes to brain development and serves as the CSF-blood barrier. Prior studies have identified transporters on the epithelial cells that transport water and ions from the blood vasculature to the ventricles and tight junctions involved in the CSF-blood barrier. Yet, how the ChP epithelial cells control brain physiology remains unresolved. We use zebrafish to provide insights into the physiological roles of the ChP. Upon histological and transcriptomic analyses, we identify that the zebrafish ChP is conserved with mammals and expresses transporters involved in CSF secretion. Next, we show that the ChP epithelial cells secrete proteins into CSF. By ablating the ChP epithelial cells, we identify a reduction of the ventricular sizes without alterations of the CSF-blood barrier. Altogether, our findings reveal that the zebrafish ChP is conserved and contributes to the size and homeostasis of the brain ventricles.

INTRODUCTION

The choroid plexus (ChP), which produces cerebrospinal fluid (CSF), is a secretory tissue located in the brain ventricles.[1] The ChP consists mainly of ciliated epithelial cells but also endothelium, immune cells, glia, and neurons.[2,3] Epithelial cells of the ChP generate CSF by transepithelial transport of electrolytes and fluid from the vasculature to the ventricles.[1] The ChP also secretes neurotrophic and growth factors into CSF that support neurodevelopment and brain homeostasis.[4,5] Thanks to tight junctions, the ChP forms the CSF-blood barrier, which is a restricted border maintaining brain homeostasis.[6] Finally, the ChP plays a role for immune surveillance.[7–9] Due to its multiple functions, alterations of the ChP are associated with various neurological diseases, including hydrocephalus[10–13] and neurodegenerative diseases.[6,14,15]

Although numerous studies have investigated the mechanisms underlying CSF secretion in physiological and pathological conditions,[1,5,14,16] how the ChP maintains the brain ventricles and regulates brain physiology remains poorly understood. We trust that zebrafish offers opportunities to address this knowledge gap due to its smaller yet conserved brain, well-characterized neural circuits, and amenable genetic tools.[17,18] Prior studies in zebrafish have mainly focused on ChP development and revealed that zebrafish have two ChPs located on the dorsal roof of the forebrain and hindbrain.[19,20] The ChPs appear during the early embryonic stage[19] and are composed of motile monociliated epithelial cells before becoming multiciliated at juvenile stages.[21,22] To date, no study has reported the physiological properties of ChP in zebrafish.

To fill this knowledge gap, we performed histological, transcriptomic, and physiological analyses of the zebrafish ChP. We first report evolutionarily conserved features of the ChP. We then developed genetic tools to label and manipulate the ChP and brain ventricles. Using these tools, we identified that the ChP regulates CSF secretion and maintains the brain ventricles.

RESULTS

The zebrafish ChP shows evolutionarily conserved anatomical characteristics

To characterize the ChP architecture, we analyzed the anatomy of the forebrain ChP (fChP) (Figures 1A–1E) and hindbrain ChP (hChP) (Figures 1F–1J) in adults. We focused on key characteristics of the ChP, previously described in mammals.

To label ChP epithelial cells, we used the *Gt(foxj1b:GFP)* line.[21–23] We observed that both ChPs are composed of a

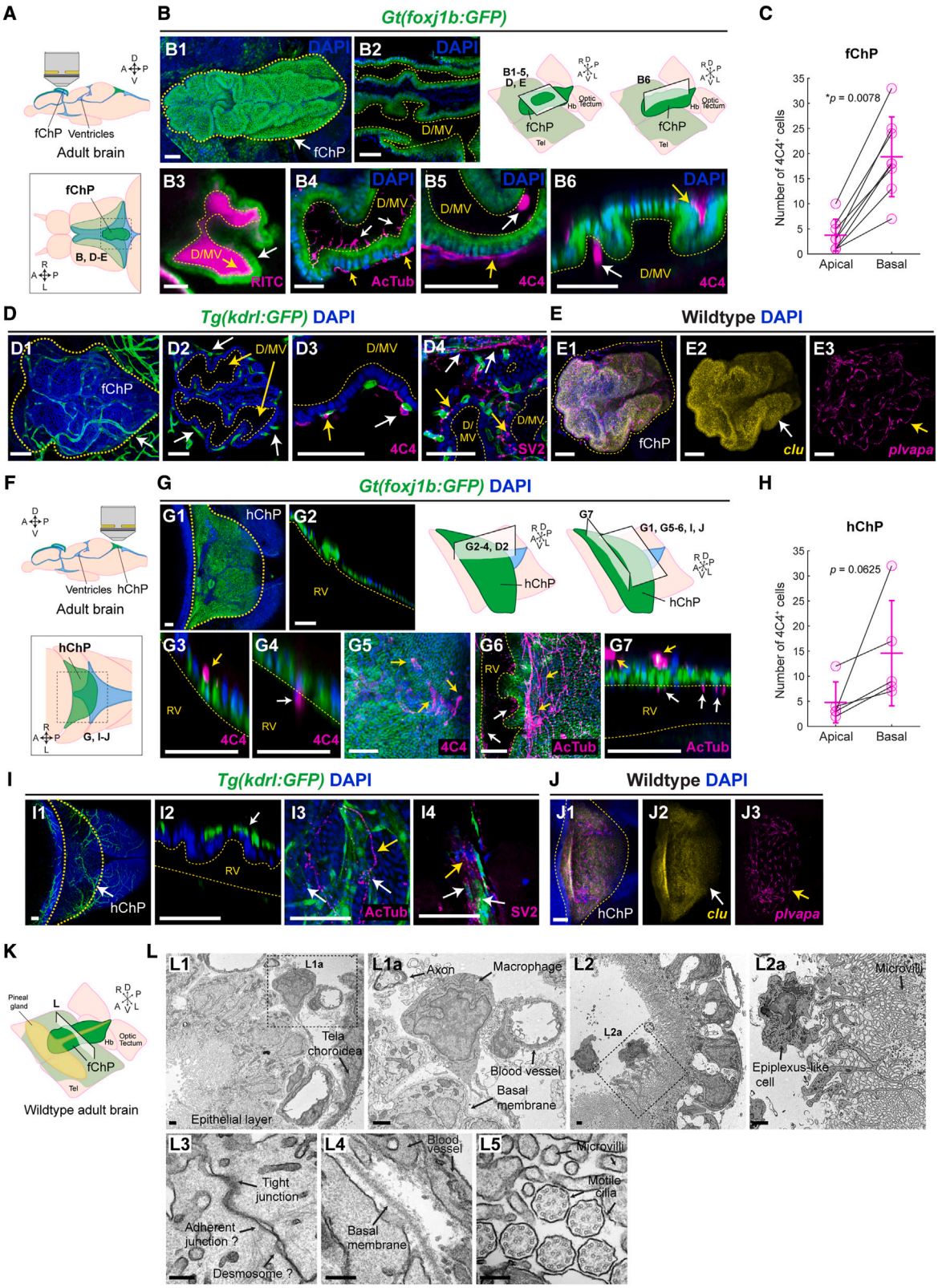

(legend on next page)

polarized monolayer of mainly *foxj1b*-expressing ciliated epithelial cells (Figures 1B and 1G). Interestingly, while the fChP is a highly folded epithelium containing multiple connected cavities filled with CSF (Figures 1B1–1B3), the hChP is arranged in a sheet of cells located above the ventricle (Figures 1G1 and 1G2).

Next, we examined the ChP vasculature using an endothelial specific line *Tg(kdrl:GFP)*.[24] Similarly to mammals, we observed blood vessels exclusively on the basolateral side of the fChP (Figure 1D) and hChP (Figure 1I) that expressed the fenestration markers *plvapa* and *plavapb* (Figures 1E, 1J, and S2).

Since the ChP is involved in immune surveillance,[7–9] we investigated the presence of macrophages using the 4C4 antibody detecting galectin 3 binding protein b.[25] We found several macrophages at the ChP basolateral side (Figures 1B5, 1B6, 1D3, 1G3, and 1G5) that contact epithelial cells (Figures 1B5 and 1G5) and blood vessels (Figure 1D3). We also identified 4C4-positive cells at the apical surfaces of both ChPs in the CSF-filled cavities (Figures 1B5, 1B6, and 1G4), which may correspond to epiplexus cells, a specialized type of macrophages in the mammalian ChP.[26,27] The number of epiplexus-like cells tended to be lower than the number of basolateral macrophages (Figures 1C and 1H).

Nerve innervations have been described in the mammalian ChP.[28–30] Using an acetylated tubulin antibody, which labels axons and cilia, we found axonal projections on the basolateral epithelia in both ChPs (Figures 1B4, 1G6, and 1G7). We also noticed SV2-labeled presynaptic vesicles in proximity to blood vessels (Figures 1D4 and 1I4) and epithelial cells (Figures 1D4 and 1I4).

To investigate the ChP ultrastructure, we performed electron microscopy of the fChP (Figures 1L and S1). We observed a polarized monolayer of epithelial cells, blood vessels, and axonal projections (Figures 1L1 and 1L1a). In the apical part, we identified cilia with a 9+2 configuration[3] (Figure 1L5) and numerous microvilli (Figures 1L2 and 1L2a), supporting a secretory role. We also observed tight junctions between epithelial cells (Figure 1L3), which are required for the CSF-blood barrier.[31] In the basolateral part, we noticed a basal membrane, blood vessels, macrophages, and axons (Figure 1L1a). We also detected an epiplexus-like cell within the CSF-filled cavity, which interacted closely with the microvilli (Figures 1L2 and L2a).

Next, we determined the anatomy of the midline tela choroidea (TC), an epithelial tissue enriched in motile ciliated epithelial cells[21] located above the telencephalic ventricle (TV). We observed that, like the ChP, the TC is a ciliated epithelial monolayer with numerous microvilli, tight junctions, fenestrated vasculature, macrophages, axonal projections, and synaptic vesicles (Figures S3B–S3F). These data show that the TC has comparable tissue characteristics to the ChP and suggest that it may play a ChP-like role in the TV.

Altogether, our analyses identified that the zebrafish ChP has evolutionarily conserved anatomical features.

The ChP develops throughout juvenile stages

We previously reported that the zebrafish ChP undergoes a transition from monociliated to multiciliated at circa 3 weeks when the brain ventricles expand significantly.[21] This motivated us to identify whether the ChP features are already established at 15–17 days post-fertilization (dpf), at the onset of multiciliation (Figure S4E1a). Notably at this stage, the fChP is organized in a flat epithelium (Figures S4B1–S4B3) and resembles more closely the hChP (Figures S4H1 and H2).

To visualize blood vessels, we microinjected Alexa 647-10 kDa dextran into the cardinal vein of *Gt(foxj1b:GFP)* (Figures S4B1 and S4H1). Like in adults, blood vessels were in the basolateral side of the TC-ChPs and expressed the fenestrated markers *plvapa/b* (Figures S4B1a and S4B1b, 3H1a, S3H1b, S4F, and S4K). We also identified fluorescent signals in the brain ventricles (Figures S4B1b and S4H1b) upon intravenous injection of Alexa 647-10 kDa.

Figure 1. The zebrafish ChP show evolutionarily conserved tissue characteristics

(A) Diagram of the fChP. Lateral (top) and dorsal (bottom) views.

(B) *Gt(foxj1b:GFP)* labels fChP epithelial cells. Max projection (B1) and single plane (B2) of the fChP showing the folded epithelium (left). Schemes representing the location of (B1)–(E3) (right). (B3) fChP injected with 70 kDa rhodamine B isothiocyanate (RITC)-dextran (magenta) in CSF. (B4) fChP labeled by acetylated-tubulin antibody marking cilia (white arrows) and axons (yellow arrows). (B5 and B6) fChP labeled with 4C4 antibody (arrows: macrophage on basal [yellow] or apical [white] side).

(C) Number of 4C4-positive cells in the apical and basal sides of the fChP.

(D) *Tg(kdrl:GFP)* labels endothelial cells in fChP. Max projection (D1) and single plane (D2–D4) of the fChP immunolabeled with 4C4 (arrows: contact with endothelial cells) (D3) and SV2 antibodies (arrows: contact with endothelial [white] or epithelial [yellow] cells) (D4).

(E) Hybridization chain reaction (HCR) of fChP for *clu* (yellow, ChP marker) and *plvapa* (magenta). Max projection. (E1–E3) Merged and individual channels.

(F) Diagram of the hChP. Lateral (top) and dorsal (bottom) views.

(G) *Gt(foxj1b:GFP)* labels hChP. Max projection (G1) and single plane (G2) of the hChP showing the sheet-like epithelium (left). Schemes representing the location of (G1)–(J3) (right). (G3–G5) hChP labeled with 4C4 antibody (arrows: macrophage on basal [yellow] or apical [white] side). (G6 and G7) hChP labeled with acetylated-tubulin antibody (yellow arrows: axons, white arrows: cilia).

(H) Number of 4C4-positive cells in the apical and basal sides of the hChP.

(I) *Tg(kdrl:GFP)*-expressing endothelial cells in hChP. Max projection (I1 and I3) and single plane (I2 and I4) of the hChP (white arrow: endothelial cells at the basal side) immunolabeled with acetylated-tubulin (arrows: contact with endothelial [white] or epithelial [yellow] cells) (I3) and SV2 antibodies (arrows: contact with endothelial [white] or epithelial [yellow] cells) (I4).

(J) HCR of the hChP with *clu* (yellow) and *plvapa* (magenta). (J1–J3) Merged and individual channels.

(K) Diagram of the fChP used for transmission electron microscopy.

(L) Images of the fChP at low (L1 and L2) and high (L1a and L2a) magnification. (L3–L5) Images of junctions (L3), basal membrane (L4), and motile cilia and microvilli (L5).

DAPI labels nuclei. Yellow dotted lines mark either the ChP or ventricles. A, anterior; P, posterior; D, dorsal; V, ventral; R, right; L, left; Hb, habenula; Tel, telencephalon. Scale bars: (A1–J3) 50 μm, (L1–L2a) 1 μm, and (L3–L5) 200 nm. Wilcoxon signed-rank test (C) ($n = 7$) (H) ($n = 5$). *$p < 0.05$.

See also Figures S1–S4.

Next, we detected 4C4-positive macrophages in both apical and basolateral sides. (Figures S4B3a–S4B3c, S4C, S4D, S4H2b, and S4J2). Using acetyl-tubulin staining, we observed cilia in the TC-ChPs, but we could not detect axonal projections near blood vessels or epithelial cells (Figures S4E1 and S4J1). Altogether, our results suggest that while all cellular components of the TC-ChPs are present in juveniles, the ChP is not fully mature, especially regarding axonal innervations.

Expression of transporter genes involved in CSF secretion is evolutionarily conserved

Prior works pinpointed a critical set of transporters involved in CSF secretion in mammals.[1,32,33] To identify whether these transporters are expressed in the zebrafish ChP, we performed bulk total RNA sequencing from adult fChPs and compared our zebrafish data with publicly available human, rat, and mouse ChP data (Figures S5 and 2).[34–36] We found 12,230 conserved genes expressed in the ChP of all 4 species, corresponding to 65%–74% of all protein-coding genes (Figures 2A, S5A, S5C, and S5D). 12–118 genes showed species-specific expression, and 314 genes were mammalian specific (Figure 2A).

Next, we evaluated the expression of transporters based on annotations from the PANTHER database. Around 80% of transporters have orthologs across all 4 species, and among these, 576 transporter genes were expressed in the ChP (Figures 2B and S5E). Their expression levels were similar across species, with the exceptions of *SEC61G*, *SLC4A5*, and *TRPM3* showing large differences in transcript per million (TPM) and ranks (Figure S5F). We next analyzed the transporters proposed to be involved in CSF secretion in mammals (Figure 2C). All seven CSF transporters were expressed in the zebrafish ChP, although the levels of *AQP1* and *SLC4A10* were lower and *SLC4A7* higher in the zebrafish (Figure 2C) compared to the mammalian ChPs. Next, we performed hybridization chain reaction and immunostaining (Figures 2D–2F) for some of the transporters. *Slc12a2* (encoding NKCC1) was dominantly expressed in the epithelial cells (Figure 2D4), whereas *aqp1a.1* was expressed mainly in some blood vessels and weakly in the epithelial cells (Figure 2D3). Both *atp1a1b* RNA (encoding for the sodium-potassium ATPase alpha1b subunit) and protein were detected in the ChP epithelial cells, primarily in their apical side (Figures 2E and 2F). Altogether, our results show that the expression of CSF transporters is evolutionarily conserved and that the zebrafish ChP has the potential to secrete CSF.

Generation of a driver line shows that *fabp7b*-expressing cells secrete proteins into CSF

Fabp7b (*fatty acid binding protein 7b*), which encodes for brain lipid-binding protein (BLBP), is strongly expressed in the ChP, based on our transcriptomic data (*fabp7b*: 2,627.58 TPMs) and a prior report.[37] To identify whether *fabp7b* could be a good ChP marker, we performed *in situ* hybridization and confirmed its strong expression in the ChPs, a subset of cells of the TC and the subcommissural organ (SCO), yet at lower levels (Figure 3A).

Next, we created a *fabp7b* knockin Gal4 driver line by inserting a Gal4 cassette in the endogenous gene (Figures 3B and S6A). By crossing the Gal4 line with the UAS effector line *Tg(uas:NTR-mCherry)*, we observed high expression of mCherry in the ChPs and some in the TC and SCO, which recapitulates our RNA expression pattern (Figures 3C and S6B). We did not observe mCherry signals in other cell types after 5 dpf (Figure S6B), although some expression was present in the hatching gland at 30 hpf (Figure S6D). Additionally, we confirmed that the BLBP antibody recognizes fabp7b in the TC and ChPs (Figure S6C), as well as fabp7a in radial glial cells.[38]

Next, by crossing *Gt(fabp7b:2A-Gal4vp16);Tg(uas:NTR-mCherry)* with *Gt(foxj1b:GFP)*, we found that *Gt(fabp7b:2A-Gal4vp16)* covers 60%–75% of the ChP (Figures S6E and S6F) but only 15%–25% of the TC and SCO (Figures S6E1, S6F, and S10A–S10C), allowing us to label and manipulate mainly the ChP epithelial cells.

Next, we tested whether *fabp7b*-expressing cells secrete proteins into CSF. We generated a transgenic line, *Tg(uas:starmaker-GFP)*, expressing starmaker, a 66 kDa secreted protein,[39] fused with GFP. By crossing *Gt(fabp7b:2A-Gal4);Tg(uas:NTR-mCherry)* with *Tg(uas:starmaker-GFP)*, we observed starmaker-GFP signals throughout the ventricles (Figures 3E1–3E5). Notably, we did not detect signals in the cytoplasm of *fabp7b*-expressing cells or elsewhere in the brain. Altogether, these data suggest that the *fabp7*-expressing cells, including the ChP epithelial cells, can secrete proteins efficiently and exclusively into the ventricle.

Ablation of *fabp7b*-expressing cells decreases the size of the brain ventricles without perturbing barrier function

To investigate the role of ChP epithelial cells in CSF production and the CSF-blood barrier, we focused our analysis on 17–18 dpf since their ChP is relatively mature and their ventricles have expanded.[21] To label CSF, we developed a strategy based on the observation that fluorescent dyes leak into the ventricles following cardinal vein injection (Figures S4B1 and S4H1). First, we confirmed that the intravenous injection genuinely labels the ventricles by injecting Alexa 647-10 kDa into *Gt(fabp7b:2A-Gal4vp16);Tg(uas:NTR-mCherry);Tg(uas:starmaker-GFP)* (Figure S7; Video S1). Confocal imaging performed 1–2 h after injection revealed clear colocalization of the fluorescent dye with starmaker-GFP throughout the ventricles (Figures S7B2 and B3), confirming the validity of our approach. Next, we examined if the intravenous injection of dyes could serve as an indicator for CSF-blood barrier function. We measured the accumulation rate of dyes of different sizes. We injected simultaneously TMR-3 kDa, Alexa 647-10 kDa and fluorescein isothiocyanate-70 kDa and imaged the brain ventricles at 30–120 min (Figure S8A). We found that the smaller dyes (3–10 kDa) tend to accumulate faster and at higher levels than the 70 kDa dye in the ventricles and parenchyma (Figures S8B–S8I). We did not identify a saturation time point, but the accumulation at 120 min was highly variable across samples. These data suggest that intravenous injection of 3–10 kDa fluorescent dyes is appropriate to measure the ventricle size and the integrity of the blood-CSF barrier in a less invasive way as compared to conventional ventricular injection.[22,40]

To determine the role of the ChP in ventricle homeostasis, we sought to ablate the ChP epithelial cells chemogenetically by the metronidazole (MTZ)-nitroreductase (NTR) system[41] (Figure 4A).

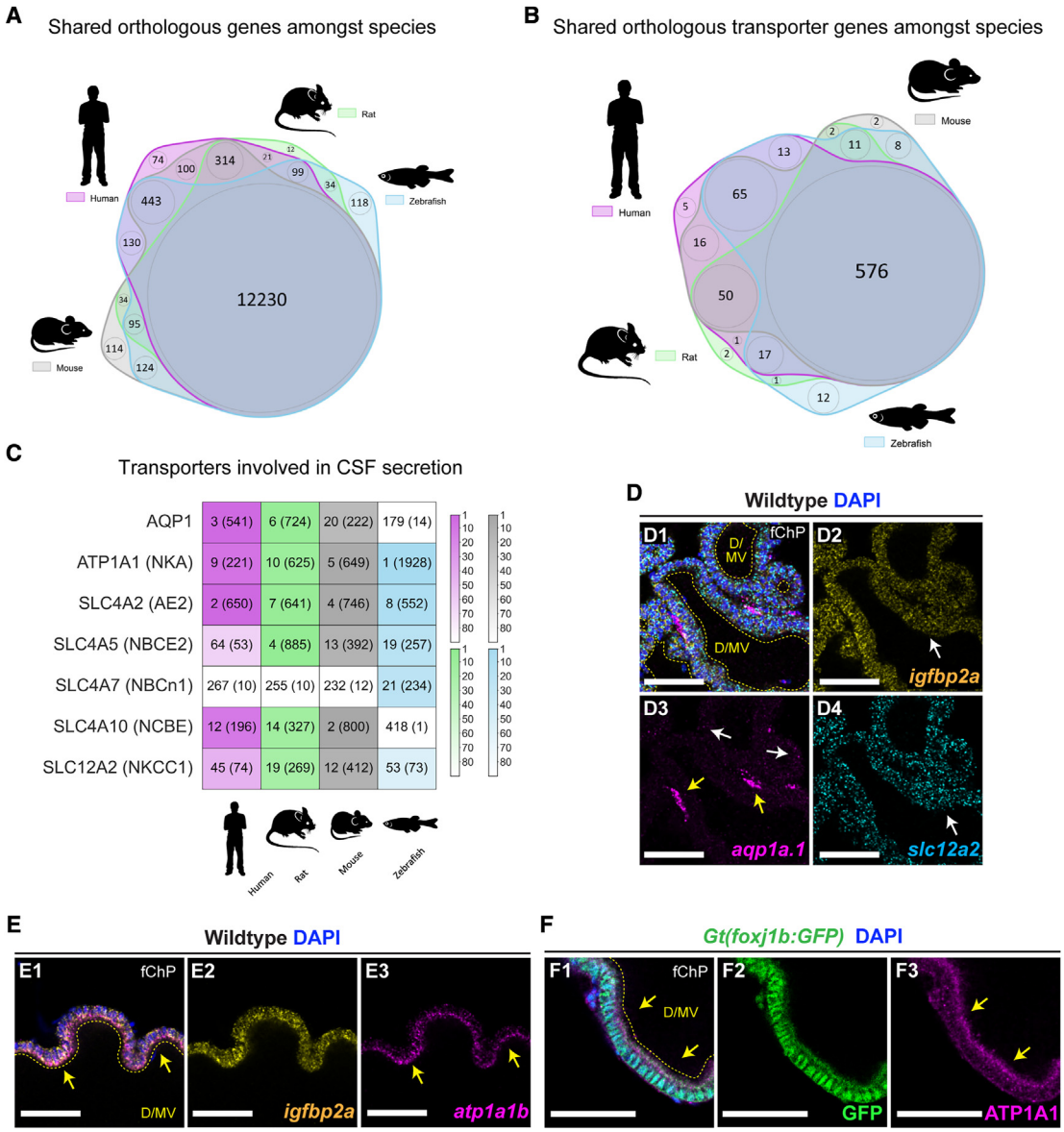

Figure 2. Expression of transporter genes is evolutionarily conserved across vertebrates

(A) Weighted Venn diagram showing protein-coding genes expressed in the ChP that have an ortholog in human, rat, mouse, and zebrafish.

(B) Weighted Venn diagram showing transporter genes expressed in the ChP that have an ortholog in all four species.

(C) Expression (rank and TPM in parentheses) of transporter genes involved in CSF secretion. Darker colors indicate higher ranks. TPMs of duplicated genes were summed into a single value.

(D and E) HCR of the fChP for *igfbp2a* (yellow, ChP marker) (D2 and E2), *aqp1a.1* (magenta) (D3), *slc12a2* (cyan) (D4), and *atp1a1b* (magenta) (E3). Single-plane images. (D1 and E1) Merged view. (D2–D4, E2, and E3) Individual channels.

(F) Staining of the fChP in *Gt(foxj1b:GFP)* for ATP1A1. Single plane. (F1–F3) Merged and individual channels. Yellow dotted lines mark the dien-/mesencephalic ventricle (D/MV). DAPI labels nuclei.

Scale bars: (D–F) 50 μm.

See also Figure S5.

We treated 14 dpf juveniles with DMSO or MTZ for 24 h. Following recovery, we injected Alexa 647-10 kDa intravenously and imaged them (Figure 4A). First, we verified the ablation efficiency (Figures 4B and 4C) by measuring the surface areas of the TC-ChPs, which express *foxj1b*-GFP. The TC and ChP sizes were reduced by 70%–77% in the ablated fish compared to two control groups: DMSO-treated NTR-mCherry positive and MTZ-treated NTR-mCherry negative (Figures 4C and 4D). Interestingly, the MTZ ablation showed similar yields in the TC and the ChP, although only around 25% of the TC expresses NTR-mCherry (Figure S6F). In contrast to the TC-ChPs, only 25% of the SCO was ablated (Figures S10D and S10E).

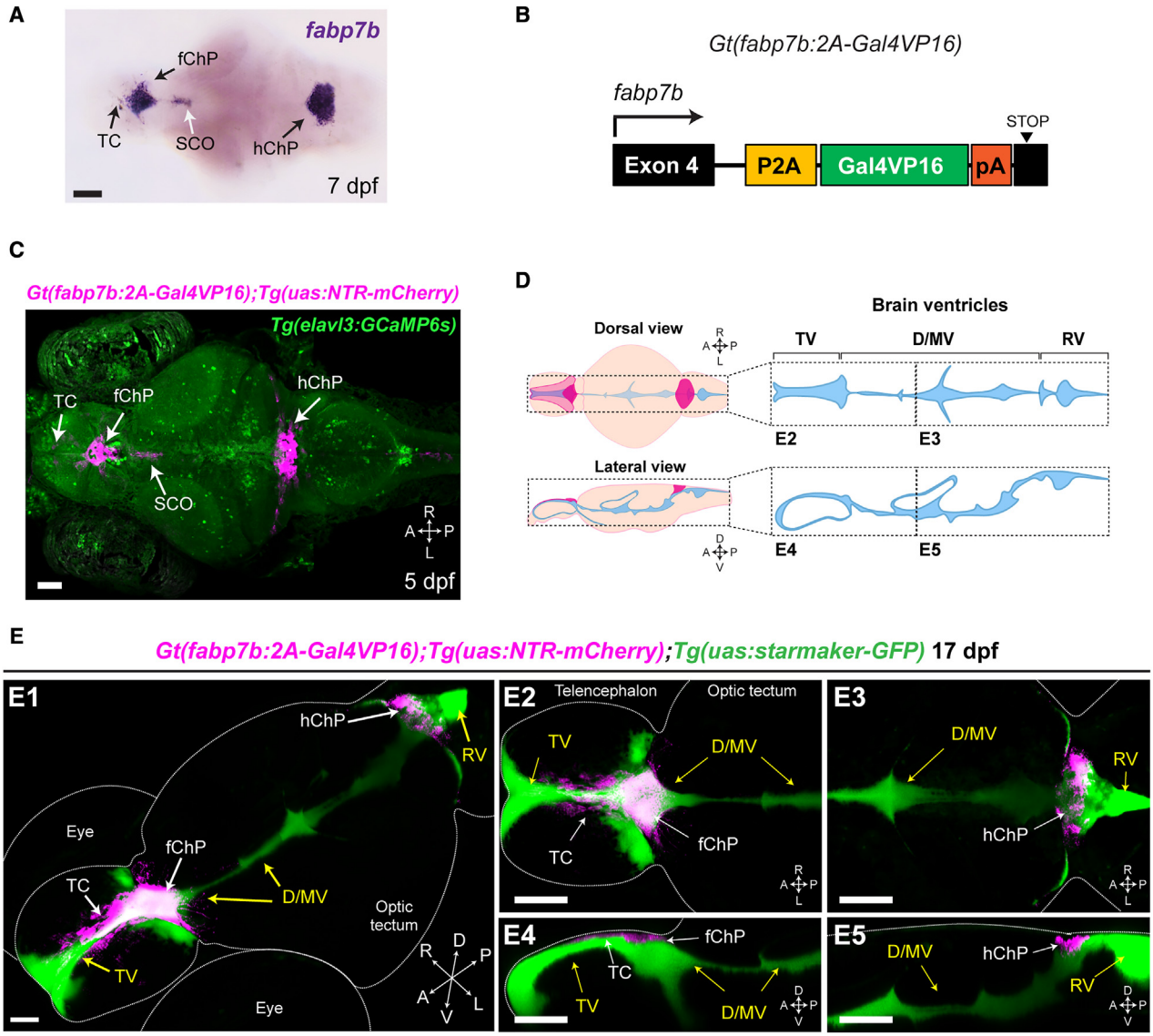

Figure 3. *Fabp7b*-expressing cells secrete proteins into the CSF and brain ventricles

(A) *fabp7b RNA* expression in the larval brain.

(B) Schematic of the Gal4 integration in *Gt(fabp7b:2A-Gal4vp16)*.

(C) Dorsal view of *Gt(fabp7b:2A-Gal4vp16);Tg(uas:NTR-mCherry);Tg(elavl3:GCaMP6s)*.

(D) Diagrams of the brain and ventricles at 17 dpf. The dotted boxes indicate the location of the images of ventricles in (E2)–(E5).

(E) Images of *Gt(fabp7b:2A-Gal4vp16);Tg(uas:NTR-mCherry);Tg(uas:starmaker-GFP)*. Dotted lines mark the brain and eyes. (E1) Reconstructed 3D image. (E2–E5) Dorsal and sagittal views of the anterior and posterior parts of the brain as indicated in (D).

TV, telencephalic ventricle; D/MV, dien-/mesencephalic ventricle; RV, rhombencephalic ventricle. A, anterior; P, posterior; D, dorsal; V, ventral; R, right; L, left. Scale bars: 50 μm.

See also Figures S6, S7, and S10.

Next, we found that all ventricles were 5%–40% smaller in the ablated fish compared to controls (Figures 4E–4G). Notably, we did not observe any differences in fish size and brain size (Figure S9). Previous studies showed that the SCO plays a role in spine morphogenesis.[42–44] We did not find any scoliosis phenotype in the ablated fish (Figure S10F).

Next, we examined the CSF-blood barrier by measuring fluorescent intensities in the CSF and parenchyma 60–100 min post-Alexa 647-10 kDa injection (Figure 5A) based on the results of the multidye experiment (Figure S8). We did not detect notable difference between control and ablated fish (Figures 5B and S11), suggesting that the brain barriers might be unaffected.

To further characterize the barrier integrity, we labeled tight junctions using a claudin 5 (Cldn5) antibody (Figure 5D). Cldn5 expression was maintained in the TC-ChP (Figures 5D3 and 5D6), although the cell number was reduced,

CellPress
OPEN ACCESS

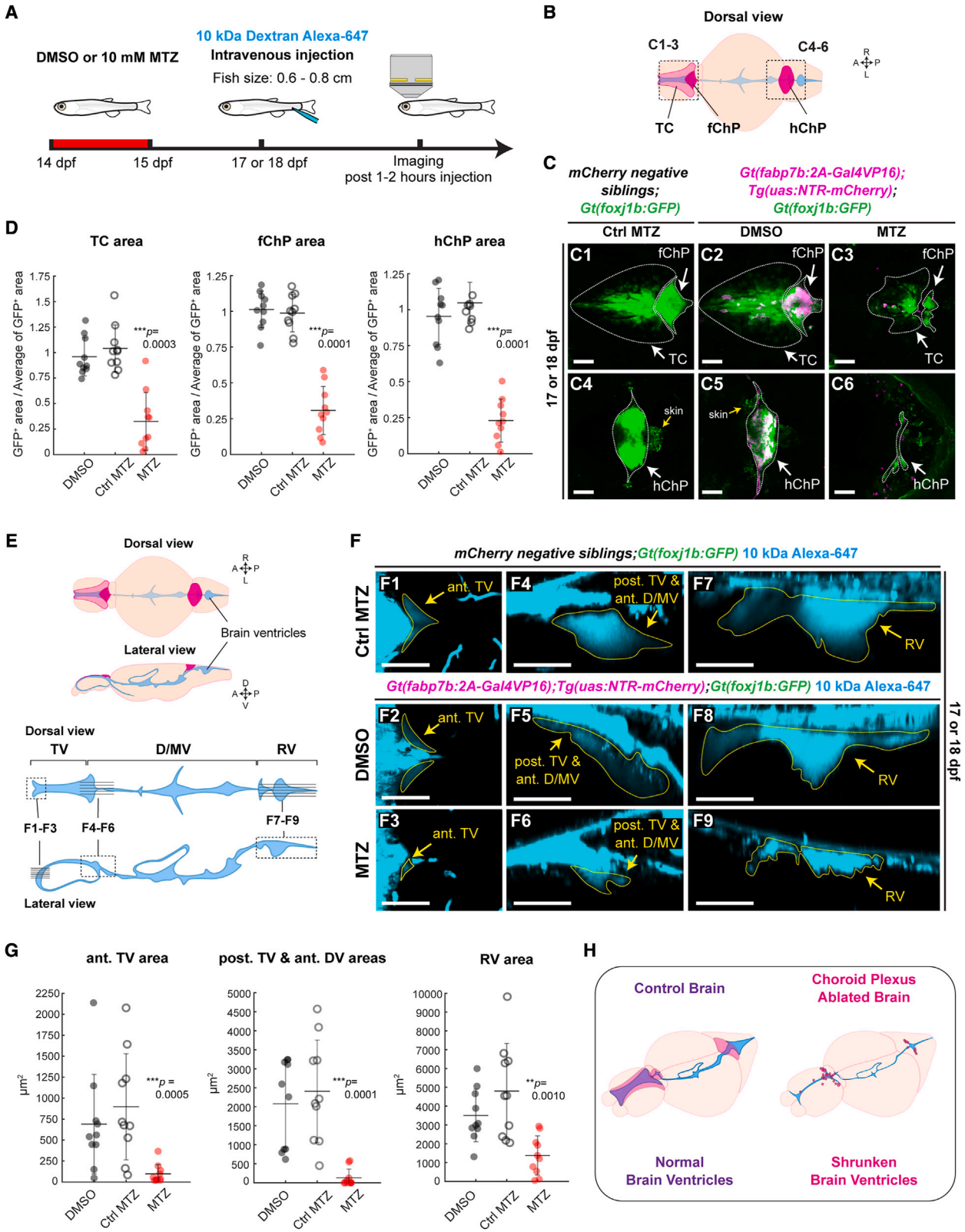

(legend on next page)

and cells displayed altered morphologies, especially in the TC (Figure 5D3).

Next, we performed electron microscopy of the juvenile fChP (Figures 5E and 5F). We confirmed that the juvenile ultrastructure in controls was similar to the adult (Figures 5E1–5E5). In the ablated fish, we observed variable phenotypes. Two ablated fish had relatively normal cuboidal cells with tight junctions and highly folded basal membranes (Figures 5F2 and 5F5), indicating that the basal membrane remains after cell loss. Only one sample had microvilli and motile cilia (Figures 5F1, 5F3, and 5F4). The third sample showed a thin cell layer that retained cellular junctions (Figure 5F6). Given that the tight junctions are maintained upon ablation, our data suggest that the barrier function remains unaltered.

Altogether, our findings identify a major role of the *fabp7b*-expressing cells and the ChP in maintaining ventricular volume, most probably through its role in CSF secretion (Figure 4H).

DISCUSSION

By performing anatomical, molecular, and physiological analyses of the zebrafish ChP, our study highlights the evolutionary conservation of the ChP and provides a deeper mechanistic understanding of ChP function.

In mammals, each ventricle has one ChP, with a total of four. In zebrafish, there are only two ChPs described based on anatomical and gene expression profiles.[19,20] Since the fChP is located next to the pineal gland, the habenula, and the SCO,[20] the fChP might correspond to the 3rd ventricle in mammals. Further gene expression analysis is, however, required to make better comparisons across species. Interestingly, the fChP, but not the hChP, folds into a complex 3D structure during the juvenile stage when the fChP expands steadily. It is not clear why only the fChP changes its shape and not the hChP. One possibility is that these folds increase the surface area to secrete more CSF in a confined area. However, it was shown that the most active ChP in mammals is in the 4th ventricle and not the 3rd.[1,45–47] It remains unclear why zebrafish do not have a ChP in the telencephalon. We show here that the TC and ChP share similar cellular features. Formally, the TC refers to a primordium of the ChP in the developing mammalian brain. It has also been used to designate a thin ventricular layer with motile ciliated cells[21] that covers the dorsal telencephalon in ray-finned fishes.[48–50] Based on our data, we suggest that the TC may have ChP-like functions.

We identified that the transcriptomes of the vertebrate ChPs are well conserved. The transporters proposed to be involved in CSF secretion in mammals are also expressed in zebrafish, which underscores the CSF-secreting ability of the zebrafish ChP. We noticed that the expression levels of some genes are different between species, including *transthyretin*, which is very low in zebrafish (0.36 TPMs) as compared to mammals (>239,000 TPMs). Notably, the expression levels of some transporter genes were slightly different, which may result in distinct ion or solute levels in CSF across species. The precise ion concentration in zebrafish CSF is currently unknown, yet artificial CSFs used in laboratories are generally slightly different for mammals and fish.[51,52] Comparing CSF properties across species may reveal knowledge on the mechanisms of brain homeostasis.

The development of genetic tools to manipulate the ChP in a time-specific manner is a game changer. Until now, it has been challenging to specifically target the ChP using genetics, and often, researchers have used the adeno-associated virus (AAV) 2/5 serotype, which preferentially targets the ChP in rodents.[53–57] Unfortunately, AAVs are not applicable in zebrafish. Here, we generated a versatile genetic tool allowing us to investigate and manipulate the ChP in zebrafish. *Fabp7b* is mainly expressed in the ChP, while its ortholog *fabp7a* is expressed in radial glia cells.[38] Based on our transcriptomics analysis, it appears that *Fabp7* is lowly expressed in mammalian ChPs (0.51–3.37 TPMs). Given its expression in neuronal progenitors,[58,59] *fabp7* may not serve as a good marker for the mammalian ChP.

Using these tools, we were able to start resolving CSF dynamics *in vivo*. We were successful at labeling the brain ventricles with a fluorescent protein using *Tg(uas:starmaker-GFP)*. In most studies, dyes or proteins are injected into the ventricles to visualize CSF.[22,60,61] This is, however, invasive and can disturb the ventricles by inducing inflammation or changing the volume. Being able to measure the morphology and size of the ventricles in a non-invasive manner will open possibilities to study CSF-associated diseases like hydrocephalus. Yet, precise

Figure 4. *Fabp7b*-expressing cells are required for the maintenance of the ventricular volume

(A) Experimental scheme used for measuring ventricular size and blood-CSF barrier integrity after ablation.

(B) Diagram of the juvenile brain with insets indicating the location of (C1)–(C6).

(C) Max projection images of the TC, fChP, and hChP in control (C1, C2, C4, and C5) and ablated fish (C3 and C6).

(D) Quantification of the TC, fChP, and hChP areas in control (DMSO and CtrlMTZ) and ablated fish (MTZ). n =10. The TC and ChP sizes are shown as normalized GFP$^+$ ratio (mean ± standard deviation). p values from post hoc analysis: TC area: DMSO vs. MTZ, $^{**}p = 0.0055$; CtrlMTZ vs. MTZ, $^{***}p = 0.0005$. fChP area: DMSO vs. MTZ, $^{***}p = 0.0002$; CtrlMTZ vs. MTZ, $^{***}p = 0.0007$. hChP area: DMSO vs. MTZ, $^{**}p = 0.0012$; CtrlMTZ vs. MTZ, $^{***}p = 0.0001$.

(E) Diagrams of the juvenile brain (top) and ventricles (bottom). Projections of 6 horizontal slices in (F1)–(F3), 5 sagittal slices in (F4)–(F6), and 5 sagittal slices in (F7)–(F9).

(F) Horizontal (F1–F3) and sagittal (F4–F6 and F7–F9) views of the ventricles following 10 kDa Alexa 647 injection in control (F1, F2, F4, F5, F7, and F8) and ablated fish (F3, F6, and F9). Ventricles are highlighted with dotted yellow lines.

(G) Quantification of the anterior (ant.) TV, posterior (post.) TV, and ant. D/MV and RV areas in the control (DMSO and CtrlMTZ) and ablated fish (MTZ). n = 10. p values from post hoc analysis: ant. TV area: DMSO vs. MTZ, $^{**}p = 0.0077$; CtrlMTZ vs. MTZ, $^{***}p = 0.0008$. post. TV and ant. D/MV areas: DMSO vs. MTZ, $^{***}p = 0.0009$; CtrlMTZ vs. MTZ, $^{***}p = 0.0003$. RV area: DMSO vs. MTZ, $^{*}p = 0.0124$; CtrlMTZ vs. MTZ, $^{**}p = 0.0015$.

(H) Diagrams of the brains in the control and ablated fish.

Kruskal-Wallis test. The p values on the graph are the results from Kruskal-Wallis test. $^{**}p < 0.01$, $^{***}p < 0.001$. TV, telencephalic ventricle; D/MV, dien-/mesencephalic ventricle; RV, rhombencephalic ventricle. A, anterior; P, posterior; D, dorsal; V, ventral; R, right; L, left. Scale bars: 50 μm.

See also Figures S8–S10.

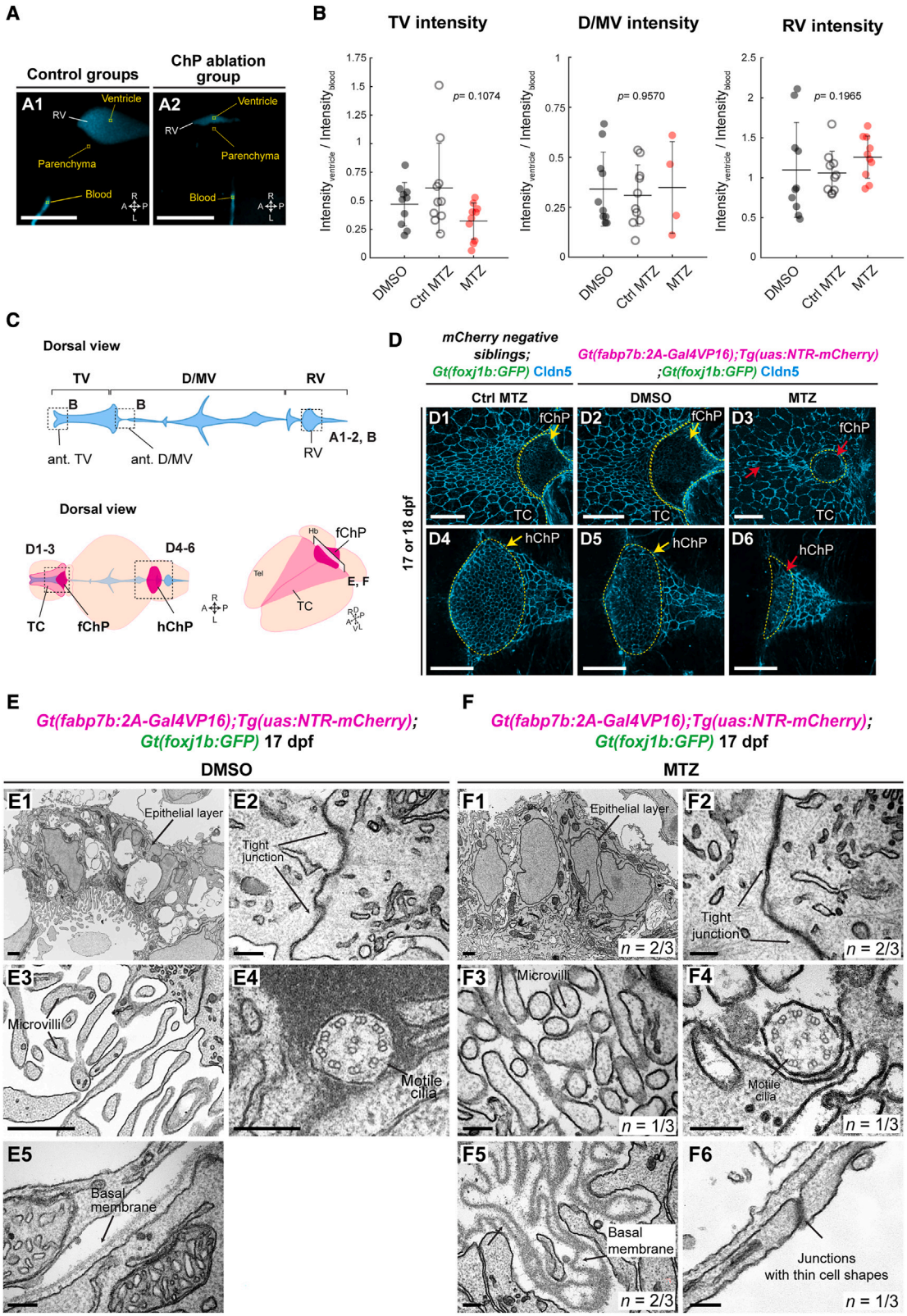

(legend on next page)

comparisons of the dynamics of various types of dyes and transgenically encoded proteins in the CSF are required to identify the most physiological approaches.

We showed that intravenous injection of fluorescent dyes labels the ventricles in a time- and size-dependent manner and allows investigation of the CSF-blood barrier integrity. It is not clear how the dyes penetrate the ventricle in the control conditions. A study identified that both the blood-brain and blood-CSF barriers were more permeable upon loss of the cldn5 in zebrafish.[62] Due to very low fluorescence intensities in the parenchyma, the dyes might not go through the blood-brain barrier but rather through the leaky circumventricular organs, such as the pituitary, which has fenestrated capillaries.[63]

In our study, we showed that ablation of *fabp7b*-expressing cells reduces the size of the brain ventricles. We suggest that reduced CSF secretion following loss of ChP epithelial cells underlies the shrunken ventricles, supporting a pivotal role for the ChP in CSF secretion.[1,64] It is expected that the amount of CSF and thereby the ventricular volume are maintained through balanced CSF secretion and clearance.[16] By reducing CSF production in the ablated fish, this would lead to a disturbed balance and a loss of the hydrostatic pressure necessary to maintain the ventricular sizes. There have been reports of extrachoroidal CSF production.[65,66] Given the major reduction of ventricles in ablated fish, these sources may contribute minimally at the investigated time point. CSF clearance pathways are poorly characterized in zebrafish. Hence, it is not possible to investigate whether CSF clearance is affected upon ablation. The ablation also affects, to a lesser extent, the SCO, which secretes SCO-spondin, the main component of the Reissner's fiber involved in spine morphogenesis in zebrafish.[43,44] SCO-spondin knockout mice have small brain ventricles with mild spine deformation,[42] suggesting that the SCO might also influence the ventricle size. Since our ablation partially affects the SCO, we cannot conclude that the reduced ventricles relate only to the TC/ChP and not to the SCO.

Taken together, our experiments provide valid proof that *fabp7*-expressing cells, most probably in the ChPs, are involved in CSF secretion, and thereby maintain ventricular volume. A preprint identified that the ablation of ChP epithelial cells also reduced CSF volume in mice.[67] This report aligns well with our data and further indicates that our observations are evolutionarily conserved.

Despite a loss of circa 70% of the epithelial cells in the TC-ChPs, we did not observe a disruption of the CSF-blood brain barrier. Cell extrusion, which removes apoptotic cells out of epithelial tissues,[68] could keep ChP integrity and sustain CSF-blood barrier function. In fact, we have observed that after ablation, cells often display abnormal shapes, yet by maintaining their tight junctions, they retain barrier function.

Altogether, the results of our work provide strong evidence that the ChP and ventricular system are conserved across vertebrates and that the ChP serves to secrete CSF also in zebrafish. Our findings thus position the zebrafish as a suitable animal model for disease modeling and open avenues for unraveling insights on the impact of the ChP and CSF on brain development and physiology in health and disease.

Limitations of the study

Prior work in rodents using bulk and single-cell transcriptomics revealed differences in gene expression between the different ChPs, especially the lateral and 4th ventricle ChP,[69] during developmental stages[2] and across sexes.[36] We investigated only the adult fChP from pooled males and females by RNA sequencing. Performing a more precise analysis of the transcriptome of the TC and the two ChPs throughout development and across sexes will allow us to better identify the mammalian counterpart of each zebrafish ChP.

Our *fabp7b:gal4* line is the most specific Gal4 driver line currently available in the zebrafish community for the ChP. Yet, we observed a mild expression in a few cells of the TC and SCO. Developing more specific genetic tools to label and manipulate solely the ChP will be useful for future studies.

STAR★METHODS

Detailed methods are provided in the online version of this paper and include the following:

- KEY RESOURCES TABLE
- RESOURCE AVAILABILITY
  - Lead contact
  - Materials availability
  - Data and code availability
- EXPERIMENTAL MODEL AND STUDY PARTICIPANT DETAILS
  - Zebrafish maintenance and strains
  - Generation of *Gt(fabp7b:2A-Gal4vp16)*^{FRZC1104} knock-in zebrafish
  - Generation of *Tg(uas:starmaker-GFP)*^{nw22Tg} line
- METHOD DETAILS
  - Immunohistochemistry and confocal microscope imaging
  - Brain ventricle injection and confocal microscope imaging
  - Hybridization chain reaction (HCR) and confocal microscope imaging
  - Transmission electron microscopy
  - Total RNA sequencing and transcriptomic analysis

Figure 5. The brain barrier is maintained in the ablated zebrafish

(A) Representative images showing how fluorescent intensities of blood plasma, brain parenchyma, and ventricle were measured in the rhombencephalon in control (A1) and ablated fish (A2).

(B) Fluorescent intensities in the ventricles in control (DMSO, CtrlMTZ) and ablated fish (MTZ). Statistical analysis: $n = 10$ except for D/MV ablated group, where $n = 4$ due to the collapse of the ventricle. Kruskal-Wallis test, $p > 0.05$.

(C) Diagrams showing the location of (A)–(F).

(D) Cldn5 immunostainings of TC, fChP, and hChP in control (D1, D2, D4, and D5) and ablated fish (D3 and D6). Max projections. $n > 4$.

(E and F) Transmission electron microscope images of the fChP in control (E) and ablated fish (F). (E1 and F1) Low- (E2–E4 and F2–F6) and high-magnification (E2, F2, and F6) images of junctions, microvilli (E3 and F3), basal membranes (E5 and F5), and motile cilia (E4 and F4).

TV, telencephalic ventricle; D/MV, dien-/mesencephalic ventricle; RV, rhombencephalic ventricle; A, anterior; P, posterior; D, dorsal; V, ventral; R, right; L, left. Scale bars: (D) 50 μm, (E1, E3, and F1) 1 μm, and (E2–E5 and F2–F6) 200 nm.

See also Figures S11 and S12.

- Cloning zebrafish *fabp7b* and whole mount RNA *in situ* hybridization
- Metronidazole treatment
- Intravenous injection and wholemount zebrafish *in vivo* live imaging
- Whole body images of zebrafish juveniles
- Imaging processing

- QUANTIFICATION AND STATISTICAL ANALYSIS
  - Quantification of 4C4 positive cell numbers of in the tela choroidea, choroid plexus
  - Quantification of NTR-mCherry expression in the tela choroidea, choroid plexus and subcommissural organ
  - Quantification of the size of brain ventricles on confocal images
  - Quantification of the fluorescent intensities on confocal images
  - Quantification of the brain parenchyma and fish size on confocal images

SUPPLEMENTAL INFORMATION

Supplemental information can be found online at https://doi.org/10.1016/j.celrep.2024.114331.

ACKNOWLEDGMENTS

We thank the Fluorescent Reporter Zebrafish Cooperation Center (FRZCC), Republic of Korea, for the *FRZCC1104* line; Valérie Wittamer for the 4C4 antibody; Sebastian Gerety for the pUAS-Self vector; Jakob Mørkved Stenersen for the initial nitroreductase optimization; and the fish facility staff and all members of the Jurisch-Yaksi/Yaksi laboratories for their feedback. BioRender was used for illustrations. This work was supported by The Research Council of Norway (314189) to N.J.-Y.; Deutsche Forschungsgemeinschaft (DFG, Germany Research Foundation), FOR5547 - Project-ID 503306912 to N.J.-Y.; a National Research Foundation of Korea grant funded by the Korea government (MSIT) (2022R1A2C1091336) to H.-C.P.; the Lundbeck Foundation (to N.M.; R276-2018-403); the Fondation ARC pour la Recherche sur le Cancer (PJA2018208167 to M.F., A2011 Postdoctoral fellowship to M.P.); the Human Frontiers Science Program (CDA00036/2010 to M.F.); and the Canceropôle PACA (Emergence 2024 to M.F.).

AUTHOR CONTRIBUTIONS

Conceptualization, N.J.-Y., I.J., N.M., S.N.A., and M.F.; methodology, I.J., S.N.A., L.H., M.P., Y.S., and M.F.; formal analysis, I.J., N.J.-Y., and S.N.A.; investigation, I.J., S.N.A., N.J.-Y., and L.H.; resources, N.J.-Y., H.-C.P., M.F., and N.M.; data curation, I.J., N.J.-Y., and S.N.A.; writing – original draft, I.J. and N.J.-Y.; writing – review & editing, all authors; visualization, I.J., N.J.-Y., and S.N.A.; supervision, N.J.-Y., H.-C.P., N.M., and M.F.; funding acquisition, N.J.-Y., H.-C.P., N.M., M.F., and M.P.

DECLARATION OF INTERESTS

The authors declare no competing interests.

Received: November 14, 2023
Revised: April 24, 2024
Accepted: May 22, 2024
Published: June 5, 2024

REFERENCES

1. MacAulay, N., Keep, R.F., and Zeuthen, T. (2022). Cerebrospinal fluid production by the choroid plexus: a century of barrier research revisited. Fluids Barriers CNS *19*, 26.
2. Dani, N., Herbst, R.H., McCabe, C., Green, G.S., Kaiser, K., Head, J.P., Cui, J., Shipley, F.B., Jang, A., Dionne, D., et al. (2021). A cellular and spatial map of the choroid plexus across brain ventricles and ages. Cell *184*, 3056–3074.e21. https://doi.org/10.1016/j.cell.2021.04.003.
3. Ho, K.H., Candat, A., Scarpetta, V., Faucourt, M., Weill, S., Salio, C., D'Este, E., Meschkat, M., Wurm, C.A., Kneussel, M., et al. (2023). Choroid plexuses carry nodal-like cilia that undergo axoneme regression from early adult stage. Dev. Cell *58*, 2641–2651.e6. https://doi.org/10.1016/j.devcel.2023.10.003.
4. Lun, M.P., Monuki, E.S., and Lehtinen, M.K. (2015). Development and functions of the choroid plexus-cerebrospinal fluid system. Nat. Rev. Neurosci. *16*, 445–457. https://doi.org/10.1038/nrn3921.
5. Saunders, N.R., Dziegielewska, K.M., Fame, R.M., Lehtinen, M.K., and Liddelow, S.A. (2023). The choroid plexus: a missing link in our understanding of brain development and function. Physiol. Rev. *103*, 919–956. https://doi.org/10.1152/physrev.00060.2021.
6. Solar, P., Zamani, A., Kubickova, L., Dubovy, P., and Joukal, M. (2020). Choroid plexus and the blood-cerebrospinal fluid barrier in disease. Fluids Barriers CNS *17*, 35. https://doi.org/10.1186/s12987-020-00196-2.
7. Cui, J., Shipley, F.B., Shannon, M.L., Alturkistani, O., Dani, N., Webb, M.D., Sugden, A.U., Andermann, M.L., and Lehtinen, M.K. (2020). Inflammation of the Embryonic Choroid Plexus Barrier following Maternal Immune Activation. Dev. Cell *55*, 617–628.e6. https://doi.org/10.1016/j.devcel.2020.09.020.
8. Kunis, G., Baruch, K., Rosenzweig, N., Kertser, A., Miller, O., Berkutzki, T., and Schwartz, M. (2013). IFN-gamma-dependent activation of the brain's choroid plexus for CNS immune surveillance and repair. Brain *136*, 3427–3440. https://doi.org/10.1093/brain/awt259.
9. Shipley, F.B., Dani, N., Xu, H., Deister, C., Cui, J., Head, J.P., Sadegh, C., Fame, R.M., Shannon, M.L., Flores, V.I., et al. (2020). Tracking Calcium Dynamics and Immune Surveillance at the Choroid Plexus Blood-Cerebrospinal Fluid Interface. Neuron *108*, 623–639.e10. https://doi.org/10.1016/j.neuron.2020.08.024.
10. Ben-Shoshan, S.D., Lolansen, S.D., Mathiesen, T.I., and MacAulay, N. (2023). CSF hypersecretion versus impaired CSF absorption in posthemorrhagic hydrocephalus: a systematic review. Acta Neurochir. *165*, 3271–3287. https://doi.org/10.1007/s00701-023-05746-9.
11. Karimy, J.K., Zhang, J., Kurland, D.B., Theriault, B.C., Duran, D., Stokum, J.A., Furey, C.G., Zhou, X., Mansuri, M.S., Montejo, J., et al. (2017). Inflammation-dependent cerebrospinal fluid hypersecretion by the choroid plexus epithelium in posthemorrhagic hydrocephalus. Nat. Med. *23*, 997–1003. https://doi.org/10.1038/nm.4361.
12. Lolansen, S.D., Rostgaard, N., Barbuskaite, D., Capion, T., Olsen, M.H., Norager, N.H., Vilhardt, F., Andreassen, S.N., Toft-Bertelsen, T.L., Ye, F., et al. (2022). Posthemorrhagic hydrocephalus associates with elevated inflammation and CSF hypersecretion via activation of choroidal transporters. Fluids Barriers CNS *19*, 62. https://doi.org/10.1186/s12987-022-00360-w.
13. Hochstetler, A., Raskin, J., and Blazer-Yost, B.L. (2022). Hydrocephalus: historical analysis and considerations for treatment. Eur. J. Med. Res. *27*, 168. https://doi.org/10.1186/s40001-022-00798-6.
14. Kaur, C., Rathnasamy, G., and Ling, E.A. (2016). The Choroid Plexus in Healthy and Diseased Brain. J. Neuropathol. Exp. Neurol. *75*, 198–213. https://doi.org/10.1093/jnen/nlv030.
15. Liu, R., Zhang, Z., Chen, Y., Liao, J., Wang, Y., Liu, J., Lin, Z., and Xiao, G. (2022). Choroid plexus epithelium and its role in neurological diseases. Front. Mol. Neurosci. *15*, 949231. https://doi.org/10.3389/fnmol.2022.949231.
16. Bothwell, S.W., Janigro, D., and Patabendige, A. (2019). Cerebrospinal fluid dynamics and intracranial pressure elevation in neurological diseases. Fluids Barriers CNS *16*, 9. https://doi.org/10.1186/s12987-019-0129-6.
17. Wyatt, C., Bartoszek, E.M., and Yaksi, E. (2015). Methods for studying the zebrafish brain: past, present and future. Eur. J. Neurosci. *42*, 1746–1763. https://doi.org/10.1111/ejn.12932.

18. Jurisch-Yaksi, N., Yaksi, E., and Kizil, C. (2020). Radial glia in the zebrafish brain: Functional, structural, and physiological comparison with the mammalian glia. Glia *68*, 2451–2470. https://doi.org/10.1002/glia.23849.

19. Garcia-Lecea, M., Kondrychyn, I., Fong, S.H., Ye, Z.R., and Korzh, V. (2008). In vivo analysis of choroid plexus morphogenesis in zebrafish. PLoS One *3*, e3090. https://doi.org/10.1371/journal.pone.0003090.

20. Korzh, V. (2023). Development of the brain ventricular system from a comparative perspective. Clin. Anat. *36*, 320–334. https://doi.org/10.1002/ca.23994.

21. D'Gama, P.P., Qiu, T., Cosacak, M.I., Rayamajhi, D., Konac, A., Hansen, J.N., Ringers, C., Acuña-Hinrichsen, F., Hui, S.P., Olstad, E.W., et al. (2021). Diversity and function of motile ciliated cell types within ependymal lineages of the zebrafish brain. Cell Rep. *37*, 109775, ARTN. https://doi.org/10.1016/j.celrep.2021.109775.

22. Olstad, E.W., Ringers, C., Hansen, J.N., Wens, A., Brandt, C., Wachten, D., Yaksi, E., and Jurisch-Yaksi, N. (2019). Ciliary Beating Compartmentalizes Cerebrospinal Fluid Flow in the Brain and Regulates Ventricular Development. Curr. Biol. *29*, 229–241.e6. https://doi.org/10.1016/j.cub.2018.11.059.

23. Tian, T., Zhao, L., Zhao, X., Zhang, M., and Meng, A. (2009). A zebrafish gene trap line expresses GFP recapturing expression pattern of foxj1b. J Genet Genomics *36*, 581–589. https://doi.org/10.1016/S1673-8527(08)60150-2.

24. Beis, D., Bartman, T., Jin, S.W., Scott, I.C., D'Amico, L.A., Ober, E.A., Verkade, H., Frantsve, J., Field, H.A., Wehman, A., et al. (2005). Genetic and cellular analyses of zebrafish atrioventricular cushion and valve development. Development *132*, 4193–4204. https://doi.org/10.1242/dev.01970.

25. Rovira, M., Miserocchi, M., Montanari, A., Hammou, L., Chomette, L., Pozo, J., Imbault, V., Bisteau, X., and Wittamer, V. (2023). Zebrafish Galectin 3 binding protein is the target antigen of the microglial 4C4 monoclonal antibody. Dev. Dynam. *252*, 400–414. https://doi.org/10.1002/dvdy.549.

26. Peters, A. (1974). The surface fine structure of the choroid plexus and ependymal lining of the rat lateral ventricle. J. Neurocytol. *3*, 99–108. https://doi.org/10.1007/BF01111935.

27. Carpenter, S.J., McCarthy, L.E., and Borison, H.L. (1970). Electron microscopic study of the epiplexus (Kolmer) cells of the cat choroid plexus. Z. Zellforsch. Mikrosk. Anat. *110*, 471–486. https://doi.org/10.1007/BF00330099.

28. Edvinsson, L., Nielsen, K.C., Owman, C., and West, K.A. (1974). Adrenergic innervation of the mammalian choroid plexus. Am. J. Anat. *139*, 299–307. https://doi.org/10.1002/aja.1001390302.

29. Lindvall, M., Alumets, J., Edvinsson, L., Fahrenkrug, J., Håkanson, R., Hanko, J., Owman, C., Schaffalitzky de Muckadell, O.B., and Sundler, F. (1978). Peptidergic (VIP) nerves in the mammalian choroid plexus. Neurosci. Lett. *9*, 77–82. https://doi.org/10.1016/0304-3940(78)90051-4.

30. Edvinsson, L., Copeland, J.R., Emson, P.C., McCulloch, J., and Uddman, R. (1987). Nerve fibers containing neuropeptide Y in the cerebrovascular bed: immunocytochemistry, radioimmunoassay, and vasomotor effects. J. Cerebr. Blood Flow Metabol. *7*, 45–57. https://doi.org/10.1038/jcbfm.1987.7.

31. Vorbrodt, A.W., and Dobrogowska, D.H. (2003). Molecular anatomy of intercellular junctions in brain endothelial and epithelial barriers: electron microscopist's view. Brain Res. Brain Res. Rev. *42*, 221–242. https://doi.org/10.1016/s0165-0173(03)00177-2.

32. Damkier, H.H., Brown, P.D., and Praetorius, J. (2013). Cerebrospinal fluid secretion by the choroid plexus. Physiol. Rev. *93*, 1847–1892. https://doi.org/10.1152/physrev.00004.2013.

33. Oernbo, E.K., Steffensen, A.B., Razzaghi Khamesi, P., Toft-Bertelsen, T.L., Barbuskaite, D., Vilhardt, F., Gerkau, N.J., Tritsaris, K., Simonsen, A.H., Lolansen, S.D., et al. (2022). Membrane transporters control cerebrospinal fluid formation independently of conventional osmosis to modulate intracranial pressure. Fluids Barriers CNS *19*, 65. https://doi.org/10.1186/s12987-022-00358-4.

34. Rodriguez-Lorenzo, S., Ferreira Francisco, D.M., Vos, R., van Het Hof, B., Rijnsburger, M., Schroten, H., Ishikawa, H., Beaino, W., Bruggmann, R., Kooij, G., and de Vries, H.E. (2020). Altered secretory and neuroprotective function of the choroid plexus in progressive multiple sclerosis. Acta Neuropathol Commun *8*, 35. https://doi.org/10.1186/s40478-020-00903-y.

35. Planques, A., Oliveira Moreira, V., Benacom, D., Bernard, C., Jourdren, L., Blugeon, C., Dingli, F., Masson, V., Loew, D., Prochiantz, A., and Di Nardo, A.A. (2021). OTX2 Homeoprotein Functions in Adult Choroid Plexus. Int. J. Mol. Sci. *22*, 8951. https://doi.org/10.3390/ijms22168951.

36. Andreassen, S.N., Toft-Bertelsen, T.L., Wardman, J.H., Villadsen, R., and MacAulay, N. (2022). Transcriptional profiling of transport mechanisms and regulatory pathways in rat choroid plexus. Fluids Barriers CNS *19*, 44. https://doi.org/10.1186/s12987-022-00335-x.

37. Liu, R.Z., Denovan-Wright, E.M., Degrave, A., Thisse, C., Thisse, B., and Wright, J.M. (2004). Differential expression of duplicated genes for brain-type fatty acid-binding proteins (fabp7a and fabp7b) during early development of the CNS in zebrafish (Danio rerio). Gene Expr. Patterns *4*, 379–387. https://doi.org/10.1016/j.modgep.2004.01.010.

38. Adolf, B., Chapouton, P., Lam, C.S., Topp, S., Tannhäuser, B., Strähle, U., Götz, M., and Bally-Cuif, L. (2006). Conserved and acquired features of adult neurogenesis in the zebrafish telencephalon. Dev. Biol. *295*, 278–293. https://doi.org/10.1016/j.ydbio.2006.03.023.

39. Sollner, C., Burghammer, M., Busch-Nentwich, E., Berger, J., Schwarz, H., Riekel, C., and Nicolson, T. (2003). Control of crystal size and lattice formation by starmaker in otolith biomineralization. Science *302*, 282–286. https://doi.org/10.1126/science.1088443.

40. Gutzman, J.H., and Sive, H. (2009). Zebrafish brain ventricle injection. J. Vis. Exp. 1218. https://doi.org/10.3791/1218.

41. Curado, S., Stainier, D.Y.R., and Anderson, R.M. (2008). Nitroreductase-mediated cell/tissue ablation in zebrafish: a spatially and temporally controlled ablation method with applications in developmental and regeneration studies. Nat. Protoc. *3*, 948–954. https://doi.org/10.1038/nprot.2008.58.

42. Xu, H., Dugué, G.P., Cantaut-Belarif, Y., Lejeune, F.X., Gupta, S., Wyart, C., and Lehtinen, M.K. (2023). SCO-spondin knockout mice exhibit small brain ventricles and mild spine deformation. Fluids Barriers CNS *20*, 89. https://doi.org/10.1186/s12987-023-00491-8.

43. Rose, C.D., Pompili, D., Henke, K., Van Gennip, J.L.M., Meyer-Miner, A., Rana, R., Gobron, S., Harris, M.P., Nitz, M., and Ciruna, B. (2020). SCO-Spondin Defects and Neuroinflammation Are Conserved Mechanisms Driving Spinal Deformity across Genetic Models of Idiopathic Scoliosis. Curr. Biol. *30*, 2363–2373.e6. https://doi.org/10.1016/j.cub.2020.04.020.

44. Troutwine, B.R., Gontarz, P., Konjikusic, M.J., Minowa, R., Monstad-Rios, A., Sepich, D.S., Kwon, R.Y., Solnica-Krezel, L., and Gray, R.S. (2020). The Reissner Fiber Is Highly Dynamic In Vivo and Controls Morphogenesis of the Spine. Curr. Biol. *30*, 2353–2362.e3. https://doi.org/10.1016/j.cub.2020.04.015.

45. Gomez, D.G., and Potts, D.G. (1981). The lateral, third, and fourth ventricle choroid plexus of the dog: a structural and ultrastructural study. Ann. Neurol. *10*, 333–340. https://doi.org/10.1002/ana.410100404.

46. Keep, R.F., Jones, H.C., and Cawkwell, R.D. (1986). A morphometric analysis of the development of the fourth ventricle choroid plexus in the rat. Brain Res. *392*, 77–85. https://doi.org/10.1016/0165-3806(86)90234-8.

47. Quay, W.B. (1966). Regional differences in metabolism and composition of choroid plexuses. Brain Res. *2*, 378–389. https://doi.org/10.1016/0006-8993(66)90007-2.

48. Nieuwenhuys, R. (2011). The development and general morphology of the telencephalon of actinopterygian fishes: synopsis, documentation

and commentary. Brain Struct. Funct. *215*, 141–157. https://doi.org/10.1007/s00429-010-0285-6.

49. Folgueira, M., Bayley, P., Navratilova, P., Becker, T.S., Wilson, S.W., and Clarke, J.D.W. (2012). Morphogenesis underlying the development of the everted teleost telencephalon. Neural Dev. *7*, 32. https://doi.org/10.1186/1749-8104-7-32.
50. Porter, B.A., and Mueller, T. (2020). The Zebrafish Amygdaloid Complex - Functional Ground Plan, Molecular Delineation, and Everted Topology. Front. Neurosci. *14*, 608. https://doi.org/10.3389/fnins.2020.00608.
51. (2017). Artificial Cerebrospinal Fluid (ACSF) (1x). Cold Spring Harb. Protoc. *2017*. https://doi.org/10.1101/pdb.rec094359.
52. Jeong, I., Hansen, J.N., Wachten, D., and Jurisch-Yaksi, N. (2022). Measurement of ciliary beating and fluid flow in the zebrafish adult telencephalon. STAR Protoc. *3*, 101542. https://doi.org/10.1016/j.xpro.2022.101542.
53. Haddad, M.R., Donsante, A., Zerfas, P., and Kaler, S.G. (2013). Fetal Brain-directed AAV Gene Therapy Results in Rapid, Robust, and Persistent Transduction of Mouse Choroid Plexus Epithelia. Mol. Ther. Nucleic Acids *2*, e101. https://doi.org/10.1038/mtna.2013.27.
54. Chen, X., He, Y., Tian, Y., Wang, Y., Wu, Z., Lan, T., Wang, H., Cheng, K., and Xie, P. (2020). Different Serotypes of Adeno-Associated Virus Vector- and Lentivirus-Mediated Tropism in Choroid Plexus by Intracerebroventricular Delivery. Hum. Gene Ther. *31*, 440–447. https://doi.org/10.1089/hum.2019.300.
55. Xu, H., Fame, R.M., Sadegh, C., Sutin, J., Naranjo, C., Syau, D., Cui, J., Shipley, F.B., Vernon, A., Gao, F., et al. (2021). Choroid plexus NKCC1 mediates cerebrospinal fluid clearance during mouse early postnatal development. Nat. Commun. *12*, 447. https://doi.org/10.1038/s41467-020-20666-3.
56. Jang, A., and Lehtinen, M.K. (2022). Experimental approaches for manipulating choroid plexus epithelial cells. Fluids Barriers CNS *19*, 36. https://doi.org/10.1186/s12987-022-00330-2.
57. Sadegh, C., Xu, H., Sutin, J., Fatou, B., Gupta, S., Pragana, A., Taylor, M., Kalugin, P.N., Zawadzki, M.E., Alturkistani, O., et al. (2023). Choroid plexus-targeted NKCC1 overexpression to treat post-hemorrhagic hydrocephalus. Neuron *111*, 1591–1608.e4. https://doi.org/10.1016/j.neuron.2023.02.020.
58. Kurtz, A., Zimmer, A., Schnütgen, F., Brüning, G., Spener, F., and Müller, T. (1994). The expression pattern of a novel gene encoding brain-fatty acid binding protein correlates with neuronal and glial cell development. Development *120*, 2637–2649. https://doi.org/10.1242/dev.120.9.2637.
59. Anthony, T.E., Klein, C., Fishell, G., and Heintz, N. (2004). Radial glia serve as neuronal progenitors in all regions of the central nervous system. Neuron *41*, 881–890. https://doi.org/10.1016/s0896-6273(04)00140-0.
60. Fame, R.M., Chang, J.T., Hong, A., Aponte-Santiago, N.A., and Sive, H. (2016). Directional cerebrospinal fluid movement between brain ventricles in larval zebrafish. Fluids Barriers CNS *13*, 11. https://doi.org/10.1186/s12987-016-0036-z.
61. Sweeney, A.M., Pla, V., Du, T., Liu, G., Sun, Q., Peng, S., Plog, B.A., Kress, B.T., Wang, X., Mestre, H., and Nedergaard, M. (2019). In Vivo Imaging of Cerebrospinal Fluid Transport through the Intact Mouse Skull using Fluorescence Macroscopy. J. Vis. Exp. *1234*, 1234. https://doi.org/10.3791/59774.
62. Li, Y., Wang, C., Zhang, L., Chen, B., Mo, Y., and Zhang, J. (2022). Claudin-5a is essential for the functional formation of both zebrafish blood-brain barrier and blood-cerebrospinal fluid barrier. Fluids Barriers CNS *19*, 40. https://doi.org/10.1186/s12987-022-00337-9.
63. Gordon, L., Blechman, J., Shimoni, E., Gur, D., Anand-Apte, B., and Levkowitz, G. (2019). The fenestrae-associated protein Plvap regulates the rate of blood-borne protein passage into the hypophysis. Development *146*, dev177790. https://doi.org/10.1242/dev.177790.
64. MacAulay, N., and Toft-Bertelsen, T.L. (2023). Dual function of the choroid plexus: Cerebrospinal fluid production and control of brain ion homeostasis. Cell Calcium *116*, 102797. https://doi.org/10.1016/j.ceca.2023.102797.
65. Pollay, M., and Curl, F. (1967). Secretion of cerebrospinal fluid by the ventricular ependyma of the rabbit. Am. J. Physiol. *213*, 1031–1038. https://doi.org/10.1152/ajplegacy.1967.213.4.1031.
66. Curl, F.D., and Pollay, M. (1968). Transport of water and electrolytes between brain and ventricular fluid in the rabbit. Exp. Neurol. *20*, 558–574. https://doi.org/10.1016/0014-4886(68)90109-x.
67. Taranov, A., Bedolla, A., Iwasawa, E., Brown, F.N., Baumgartner, S., Fugate, E.M., Levoy, J., Crone, S.A., Goto, J., and Luo, Y. (2024). The choroid plexus maintains ventricle volume and adult subventricular zone neuroblast pool, which facilitates post-stroke neurogenesis. Preprint at bioRxiv, 2024.01.22.575277. https://doi.org/10.1101/2024.01.22.575277.
68. Guillot, C., and Lecuit, T. (2013). Mechanics of epithelial tissue homeostasis and morphogenesis. Science *340*, 1185–1189. https://doi.org/10.1126/science.1235249.
69. Lun, M.P., Johnson, M.B., Broadbelt, K.G., Watanabe, M., Kang, Y.J., Chau, K.F., Springel, M.W., Malesz, A., Sousa, A.M.M., Pletikos, M., et al. (2015). Spatially heterogeneous choroid plexus transcriptomes encode positional identity and contribute to regional CSF production. J. Neurosci. *35*, 4903–4916. https://doi.org/10.1523/JNEUROSCI.3081-14.2015.
70. Vladimirov, N., Mu, Y., Kawashima, T., Bennett, D.V., Yang, C.T., Looger, L.L., Keller, P.J., Freeman, J., and Ahrens, M.B. (2014). Light-sheet functional imaging in fictively behaving zebrafish. Nat. Methods *11*, 883–884. https://doi.org/10.1038/nmeth.3040.
71. Lister, J.A., Robertson, C.P., Lepage, T., Johnson, S.L., and Raible, D.W. (1999). nacre encodes a zebrafish microphthalmia-related protein that regulates neural-crest-derived pigment cell fate. Development *126*, 3757–3767. https://doi.org/10.1242/dev.126.17.3757.
72. Wierson, W.A., Welker, J.M., Almeida, M.P., Mann, C.M., Webster, D.A., Torrie, M.E., Weiss, T.J., Kambakam, S., Vollbrecht, M.K., Lan, M., et al. (2020). Efficient targeted integration directed by short homology in zebrafish and mammalian cells. Elife *9*, e53968. https://doi.org/10.7554/eLife.53968.
73. Welker, J.M., Wierson, W.A., Almeida, M.P., Mann, C.M., Torrie, M.E., Ming, Z., Ekker, S.C., Clark, K.J., Dobbs, D.L., Essner, J.J., and McGrail, M. (2021). GeneWeld: Efficient Targeted Integration Directed by Short Homology in Zebrafish. Bio. Protoc. *11*, e4100. https://doi.org/10.21769/BioProtoc.4100.
74. Jao, L.E., Wente, S.R., and Chen, W. (2013). Efficient multiplex biallelic zebrafish genome editing using a CRISPR nuclease system. Proc. Natl. Acad. Sci. USA *110*, 13904–13909. https://doi.org/10.1073/pnas.1308335110.
75. Schindelin, J., Arganda-Carreras, I., Frise, E., Kaynig, V., Longair, M., Pietzsch, T., Preibisch, S., Rueden, C., Saalfeld, S., Schmid, B., et al. (2012). Fiji: an open-source platform for biological-image analysis. Nat. Methods *9*, 676–682. https://doi.org/10.1038/nmeth.2019.
76. Labun, K., Montague, T.G., Krause, M., Torres Cleuren, Y.N., Tjeldnes, H., and Valen, E. (2019). CHOPCHOP v3: expanding the CRISPR web toolbox beyond genome editing. Nucleic Acids Res. *47*, W171–W174. https://doi.org/10.1093/nar/gkz365.
77. Agetsuma, M., Aizawa, H., Aoki, T., Nakayama, R., Takahoko, M., Goto, M., Sassa, T., Amo, R., Shiraki, T., Kawakami, K., et al. (2010). The habenula is crucial for experience-dependent modification of fear responses in zebrafish. Nat. Neurosci. *13*, 1354–1356. https://doi.org/10.1038/nn.2654.
78. Rayamajhi, D., Ege, M., Ukhanov, K., Ringers, C., Zhang, Y., Jeong, I., D'Gama, P.P., Li, S.S., Cosacak, M.I., Kizil, C., et al. (2023). Foxj1 controls olfactory ciliogenesis and differentiation program of the olfactory sensory neurons. Preprint at bioRxiv. https://doi.org/10.1101/2023.05.10.540158.

79. Jeong, I., Yun, S., Shahapal, A., Cho, E.B., Hwang, S.W., Seong, J.Y., and Park, H.C. (2021). FAM19A5l Affects Mustard Oil-Induced Peripheral Nociception in Zebrafish. Mol. Neurobiol. *58*, 4770–4785. https://doi.org/10.1007/s12035-021-02449-z.

80. Kermen, F., Darnet, L., Wiest, C., Palumbo, F., Bechert, J., Uslu, O., and Yaksi, E. (2020). Stimulus-specific behavioral responses of zebrafish to a large range of odors exhibit individual variability. BMC Biol. *18*, 66. https://doi.org/10.1186/s12915-020-00801-8.

81. Kermen, F., Lal, P., Faturos, N.G., and Yaksi, E. (2020). Interhemispheric connections between olfactory bulbs improve odor detection. PLoS Biol. *18*, e3000701. https://doi.org/10.1371/journal.pbio.3000701.

82. D'Gama, P.P., and Jurisch-Yaksi, N. (2023). Methods to study motile ciliated cell types in the zebrafish brain. Methods Cell Biol. *176*, 103–123. https://doi.org/10.1016/bs.mcb.2023.01.020.

83. Hua, Y., Laserstein, P., and Helmstaedter, M. (2015). Large-volume en-bloc staining for electron microscopy-based connectomics. Nat. Commun. *6*, 7923. https://doi.org/10.1038/ncomms8923.

84. Mikula, S., and Denk, W. (2015). High-resolution whole-brain staining for electron microscopic circuit reconstruction. Nat. Methods *12*, 541–546. https://doi.org/10.1038/nmeth.3361.

85. Edgar, R., Domrachev, M., and Lash, A.E. (2002). Gene Expression Omnibus: NCBI gene expression and hybridization array data repository. Nucleic Acids Res. *30*, 207–210. https://doi.org/10.1093/nar/30.1.207.

86. Barrett, T., Wilhite, S.E., Ledoux, P., Evangelista, C., Kim, I.F., Tomashevsky, M., Marshall, K.A., Phillippy, K.H., Sherman, P.M., Holko, M., et al. (2013). NCBI GEO: archive for functional genomics data sets–update. Nucleic Acids Res. *41*, D991–D995. https://doi.org/10.1093/nar/gks1193.

87. Andrews, S. (2010). FastQC: A Quality Control Tool for High Throughput Sequence Data.

88. Bolger, A.M., Lohse, M., and Usadel, B. (2014). Trimmomatic: a flexible trimmer for Illumina sequence data. Bioinformatics *30*, 2114–2120. https://doi.org/10.1093/bioinformatics/btu170.

89. Dobin, A., Davis, C.A., Schlesinger, F., Drenkow, J., Zaleski, C., Jha, S., Batut, P., Chaisson, M., and Gingeras, T.R. (2013). STAR: ultrafast universal RNA-seq aligner. Bioinformatics *29*, 15–21. https://doi.org/10.1093/bioinformatics/bts635.

90. Li, B., and Dewey, C.N. (2011). RSEM: accurate transcript quantification from RNA-Seq data with or without a reference genome. BMC Bioinf. *12*, 323. https://doi.org/10.1186/1471-2105-12-323.

91. Cunningham, F., Allen, J.E., Allen, J., Alvarez-Jarreta, J., Amode, M.R., Armean, I.M., Austine-Orimoloye, O., Azov, A.G., Barnes, I., Bennett, R., et al. (2022). Ensembl 2022. Nucleic Acids Res. *50*, D988–D995. https://doi.org/10.1093/nar/gkab1049.

92. Kinsella, R.J., Kähäri, A., Haider, S., Zamora, J., Proctor, G., Spudich, G., Almeida-King, J., Staines, D., Derwent, P., Kerhornou, A., et al. (2011). Ensembl BioMarts: a hub for data retrieval across taxonomic space. Database *2011*, bar030. https://doi.org/10.1093/database/bar030.

93. Waskom, M.L. (2021). seaborn: statistical data visualization. J. Open Source Softw.

94. Hunter, J.D. (2007). Matplotlib: A 2D Graphics Environment. Comput. Sci. Eng. *9*, 90–95.

95. Perez-Silva, J.G., Araujo-Voces, M., and Quesada, V. (2018). nVenn: generalized, quasi-proportional Venn and Euler diagrams. Bioinformatics *34*, 2322–2324. https://doi.org/10.1093/bioinformatics/bty109.

96. Mi, H., Ebert, D., Muruganujan, A., Mills, C., Albou, L.P., Mushayamaha, T., and Thomas, P.D. (2021). PANTHER version 16: a revised family classification, tree-based classification tool, enhancer regions and extensive API. Nucleic Acids Res. *49*, D394–D403. https://doi.org/10.1093/nar/gkaa1106.

97. Thisse, C., and Thisse, B. (2008). High-resolution in situ hybridization to whole-mount zebrafish embryos. Nat. Protoc. *3*, 59–69. https://doi.org/10.1038/nprot.2007.514.

98. Palumbo, F., Serneels, B., Pelgrims, R., and Yaksi, E. (2020). The Zebrafish Dorsolateral Habenula Is Required for Updating Learned Behaviors. Cell Rep. *32*, 108054. https://doi.org/10.1016/j.celrep.2020.108054.

99. O'Brown, N.M., Megason, S.G., and Gu, C. (2019). Suppression of transcytosis regulates zebrafish blood-brain barrier function. Elife *8*, e47326. https://doi.org/10.7554/eLife.47326.

100. Preibisch, S., Saalfeld, S., and Tomancak, P. (2009). Globally optimal stitching of tiled 3D microscopic image acquisitions. Bioinformatics *25*, 1463–1465. https://doi.org/10.1093/bioinformatics/btp184.

STAR★METHODS

KEY RESOURCES TABLE

REAGENT or RESOURCE	SOURCE	IDENTIFIER
Antibodies		
4C4 antibody, mouse monoclonal	Valérie Wittamer lab (Rovira et al.[25])	RRID:AB_10013752
Acetylated tubulin antibody, Mouse monoclonal	Sigma-Aldrich	Cat# T7451; RRID: AB_609894
Fabp7 antibody, rabbit polyclonal	Millipore	Cat#ABN14; RRID:AB_10000325
SV2 antibody, mouse monoclonal	Developmental Studies Hybridoma Bank	Cat# 2315387; RRID:AB_2315387
GFP Polyclonal Antibody, Alexa Fluor™ 488	Thermo Fisher Scientific	Cat# A-21311; RRID:AB_221477
Claudin 5 (Cldn5) monoclonal antibody	Thermo Fisher Scientific	Cat# 35–2500; RRID: AB_2533200
ATP1A1 antibody (a6F)	Developmental Studies Hybridoma Bank	Cat# 528092; RRID: AB_528092
Goat anti-Mouse secondary antibody Alexa Fluor™ Plus 647	Thermo Fisher Scientific	Cat# A32728; RRID:AB_2633277
Goat anti-Rabbit secondary antibody Alexa Fluor™ Plus 647	Thermo Fisher Scientific	Cat# A32733; RRID:AB_2633282
AP-anti DIG antibody	Roche	Cat#11093274910; RRID: AB_514497
Bacterial and virus strains		
One Shot™ TOP10 Chemically Competent E. coli	Thermo Fisher Scientific	Cat# C404010
Chemicals, peptides, and recombinant proteins		
MS-222	Sigma-Aldrich	Cat# E10621-60G
Artificial fish water (AFW)	Jeong et al.[53]	N/A
Artificial cerebrospinal fluid (aCSF)	Jeong et al.[53]	N/A
70 kDa rhodamine B isothiocyanate-dextran	Sigma-Aldrich	Cat# R9379
Phosphate buffered saline (PBS)	Thermo Fisher Scientific	Cat# BR0014G
Triton X-100	Merck	Cat# 1086031000
Bovine Serum Albumin (BSA)	PanReac AppliedChem	Cat# A1391
Dimethyl sulfoxide (DMSO)	Sigma-Aldrich	Cat# D8418
Glycerol	VWR	Cat# 24387.292
Acetone	VWR	Cat# 20066.296
Acetone (anhydrous) for electron microscopy	VWR	Cat# 83683.290
Formaldehyde solution (PFA)	Sigma-Aldrich	Cat# F8775-25mL
DAPI (4′,6-Diamidino-2-Phenylindole, Dihydrochloride)	Thermo Fisher Scientific	Cat# D1306
Glutaraldehyde, 50%, EM grade aqueous	Electron Microscopy Sciences	Cat# 16320
Paraformaldehyde, reagent grade, crystaline	Sigma-Aldrich	Cat# P6148
Sodium cacodylate purum	Sigma-Aldrich	Cat# 20840
Potassium hexacyanoferrate(II) BioUltra	Sigma-Aldrich	Cat# 60279
Osmium tetroxide, Crystalline, Highest Purity, 99.95%	Electron Microscopy Sciences	Cat# 19110
Pyrogallol, ACS reagent	Sigma-Aldrich	Cat# 16040
Ethanol for electron microscopy	VWR	Cat# 20821.310
Lead Nitrate, reagent, ACS	Electron Microscopy Sciences	Cat# 17900
L-Aspartic acid, reagent grade, 98%	Sigma-Aldrich	Cat# A9256

(*Continued on next page*)

Continued

REAGENT or RESOURCE	SOURCE	IDENTIFIER
Thiocarbohydrazide, purum, for electron microscopy, ≥99.0%	Sigma-Aldrich	Cat# 88535
Uranyl Acetate	Electron Microscopy Sciences	Cat# 02624
Nuclease-Free water	Thermo Fisher Scientific	Cat# AM9930
TRIzol	Invitrogen	Cat# 15596026
RNeasy mini kit	QIAGEN	Cat#74104 (50 reactions)
RNase-Free DNase Set	QIAGEN	Cat#79254 (50 reactions)
RNAlater™	Thermo Fisher Scientific	Cat# AM0720
Phenol:Chloroform 5:1	Sigma-Aldrich	Cat# P1944
Chloroform	Sigma-Aldrich	Cat# 366919
Glycogen, RNA grade	Thermo Fisher Scientific	Cat# R0551
XbaI restriction enzyme	New England Biolabs	Cat# R0145S
SacII restriction enzyme	New England Biolabs	Cat# R0157S
CutSmart Buffer	New England Biolabs	Cat# B7204
Ethanol	Sigma-Aldrich	Cat# 110983
Methanol	Sigma-Aldrich	Cat# 106009
T7 RNA polymerase	Roche	Cat# 10881767001
SP6 RNA polymerase	Roche	Cat# 10810274001
Ribonucleoside Triphosphate Set pkg of 4 × 200 μL	Roche	Cat# 11277057001
T7 endonuclease I	New England Biolabs	Cat# M0302L
DIG RNA Labeling Mix solution	Roche	Cat# 11277073910
RNase inhibitor	Enzynomics	Cat# M007M
Formamide	Junsei	Cat# 69355S0350
SSC Buffer 20X	Sigma-Aldrich	Cat# S66
NBT/BCIP stock solution	Roche	Cat#11681451001
Metronidazole (MTZ)	Sigma-Aldrich	Cat# M1547
Dextran, Alexa Fluor™ 647; 10,000 MW (10 kDa)	Thermo Fisher Scientific	Cat# D22914
Dextran, Tetramethylrhodamine (TMR), 3000 MW, Anionic, Lysine Fixable (3 kDa)	Thermo Fisher Scientific	Cat# D3308
Fluorescein isothiocyanate (FITC)-dextran, MW 70,000 (70kDa)	Sigma-Aldrich	Cat# 90718
Proteinase K from tritirachium album	Sigma-Aldrich	Cat# P2308-25MG
Dulbecco's Phosphate Buffered Saline	Merck	Cat# 59331C
Critical commercial assays		
QIAGEN Plasmid Midi kit	QIAGEN	Cat# 12143
PureYield™ Plasmid Miniprep System	Promega	Cat# A1223
QIAprep Spin Miniprep kit (250)	QIAGEN	Cat# 27106
EMbed 812 kit for Electron Microscopy Embedding	Electron Microscopy Sciences	Cat# 14120
mMESSAGE mMACHINE™ T3 transcription kit	Thermo Fisher Scientific	Cat# AM1348
Multiplex HCRv3 reagents	Molecular Instruments	https://www.molecularinstruments.com/
Deposited data		
GEO for RNA sequencing	This paper	GEO: GSE246851
Codes for the analysis of RNA sequencing	This paper	Zenodo: https://doi.org/10.5281/zenodo.11230620
Raw images and image analysis data and codes	This paper	NIRD research data archive: https://doi.org/10.11582/2024.00088
Experimental models: Organisms/strains		
Zebrafish: *T2BGSZ10 Gt(foxj1b:GFP)*^{tsu10Gt}	Meng lab, Tsinghua University (Tian et al.[23])	ZFIN: ZDB-ALT-110301-1
Zebrafish: *Gt(fabp7b:2A-Gal4vp16)*^{FRZCC1104}	This paper	N/A

(*Continued on next page*)

Continued

REAGENT or RESOURCE	SOURCE	IDENTIFIER
Zebrafish: *Tg(uas:starmaker-GFP)^{nw22Tg}*	This paper	N/A
Zebrafish: *Tg(uas:NTR-mCherry)*	Agetsuma et al.[70]	ZFIN: ZDB-TGCONSTRCT-070314-2
Zebrafish: *Tg(kdrl:GFP)^{s843Tg}*	Beis et al.[24]	ZFIN: ZDB-ALT-050916-14
Zebrafish: *Tg(elavl3:GCaMP6s) ^{jf4Tg}*	Ahrens lab, Janelia farm (Vladimirov et al.[71])	ZFIN: ZDB-ALT-141023-1
Zebrafish: *Nacre (mitfa$^{-/-}$) ^{b692}*	Lister et al.[72]	ZFIN:ZDB-ALT-010919-2
Zebrafish: *Wildtype*	N/A	TU/AB
Oligonucleotides		
Fabp7b forward primer for cloning, 5′-GGAAATGTGACCAAACCGAC-3′	MACROGEN	N/A
Fabp7b reverse primer for cloning, 5′-TGGCCAGAAAGAAGAACAGC-3′	MACROGEN	N/A
Fabp7b sgRNA, 5′-AAGAGCCTCCACGTCCCCAA-3′	CHOPCHOP	https://chopchop.cbu.uib.no/
Fabp7b sgRNA gRNA sequence for gRNA synthesis, 5′-TAATACGACTCACTATAgGC AGTGTCGGTCATCAGCAGgttttagagctagaaatagc-3′	MACROGEN and Wierson et al.[73]	N/A
Fabp7b knockin genotyping forward primer, 5′-TGGGTTTGCAACAAGACAAGTTGG-3′	MACROGEN	N/A
Fabp7b knockin genotyping reverse primer, 5′-GGCCAGAAAGAAGAACAGCGAC-3′	MACROGEN	N/A
Fabp7b 5′ homology arm forward sequence for cloning, 5′-gcggAAACATTTAATATCTTTCTGATT TCAACTTCGATTTAGAAACTCACCTTTGGG-3′	MACROGEN	N/A
Fabp7b 5′ homology arm reverse sequence for cloning, 5′-atccCCCAAAGGTGAGTTTCTAAATC GAAGTTGAAATCAGAAAGATATTAAATGTTT-3′	MACROGEN	N/A
Fabp7b 3′ homology arm forward sequence for cloning, 5′-aagCCCTTCCCAAAGCCTATGCTTT TTCATAGGTGCGAAGAGCCTCCACGTCCC-3′	MACROGEN	N/A
Fabp7b 3′ homology arm reverse sequence for cloning, 5′-cggGGGACGTGGAGGCTCTTCGCA CCTATGAAAAAGCATAGGCTTTGGGAAGGG-3′	MACROGEN	N/A
Gal4 5′ junction reverse primer, 5′-GCCTTGATTCCACTTCTGTCA-3′	MACROGEN	Welker et al.[38] and Wierson et al.[73]
Gal4 3′ junction forward primer 5′-GCAAACGGCCTTAACTTTCC-3′	MACROGEN	Welker et al.[38] and Wierson et al.[73]
Starmaker-GFP forward primer for cloning, 5′-CTCCTCCACACGAATTCGCAAACATGC TGTCCCGGACAGTGTTTG-3′	MWG Eurofins	N/A
Starmaker-GFP reverse primer for cloning 5′-TAGTTCTAGAGGCTCGATTACTTGTAC AGCTCGTCCATGCC-3′	MWG Eurofins	N/A
Recombinant DNA		
pGEMT-fabp7b plasmid	This paper	N/A
pGTag-fabp7b-2A-gal4vp16	This paper	N/A
pGEM-T easy vector	Promega	CAT# A1360
pT3TS-nCas9n vector	Jao et al.[74]	RRID:Addgene_46757
pGTag-2A-Gal4vp16-B-actin plasmid	Wierson et al.[73]	RRID:Addgene_117817
uas:starmaker-GFP plasmid	This paper	N/A
Software and algorithms		
ImageJ/Fiji	Schindelin et al.[75]	https://imagej.net/Fiji.html#Downloads
MALTLAB 2023a	MathWorks	https://se.mathworks.com/

(*Continued on next page*)

Continued

REAGENT or RESOURCE	SOURCE	IDENTIFIER
Huygen software	Scientific Volume Imaging	https://svi.nl/Huygens-Software
Radius software version 2.0	EMSIS GmbH	https://www.emsis.eu/products/radius
All codes for transcriptomics analysis	This paper	https://doi.org/10.5281/zenodo.11230620
CHOPCHOP	Labun et al.[76]	https://chopchop.cbu.uib.no/
Other		
Thin Wall Glass Capillaries (4 in, OD 1.0 mm, Filament)	World Precision Instruments	Cat# TW100F-4
Flurodish	VWR	Cat# FD35PDL-100
Confocal microscope	Zeiss	LSM880 with Examiner Z1
20x water immersion Plan-Apochromat NA 1.0	Zeiss	421452-9880-000
20x Plan-Apochromat NA 0.8	Zeiss	420650-9901-000
Sutter Laser puller	Sutter Instrument	P-2000
Pressure injector	Eppendorf	Femtojet 4i
Ultramictrotome	Leica Microsystems	Leica EM UC7
Diamond knife	DiATOME	Ultra Diamond Knife Wet 45
Biowave Pro +	Pelco	Cat# 36700
Transmission electron microscope	JEOL	JEOL JSM-1011
NanoDrop	Thermo Fisher Scientific	ND-1000
Ni-U fluorescent microscope (Nikon) with DS-Ri2 camera	Nikon	Ni-U, DS-RiS
Stereomicroscope	Olympus	SZX7

RESOURCE AVAILABILITY

Lead contact

Further information and requests for resources and reagents should be directed to and will be fulfilled by the lead contact, Nathalie Jurisch-Yaksi (nathalie.jurisch-yaksi@ntnu.no).

Materials availability

Material generated in this paper will be shared by their creators (I.J., H.C.P: *Gt(fabp7b:2A-Gal4vp16)*^{FRZCC1104}, I.J., N.Y.J: *Tg(uas:starmaker-GFP)*^{nw22Tg}, M.F UAS:starmaker-GFP plasmid) upon request and may require completion of a material transfer agreement.

Data and code availability

- The RNA sequencing data have been deposited at GEO and are publicly available. The accession number is listed in the key resource table. Raw imaging data to generate the figures of this paper are publicly available and the DOI is listed in the key resource table.
- Codes for the analysis of RNA sequencing are deposited at Zenodo and are publicly available. All the quantifications and original codes used in the manuscript are deposited in the NIRD research data archive and are publicly available. The DOIs are listed in the key resource table.
- Any additional information required to reanalyze the data reported in this paper is available from the lead contact upon request.

EXPERIMENTAL MODEL AND STUDY PARTICIPANT DETAILS

Zebrafish maintenance and strains

The animal facilities and maintenance of zebrafish, Danio rerio, were approved by the Norwegian Food Safety Authority and the Korea Disease Control and Prevention Agency. All the procedures were performed on zebrafish at different developmental stages post fertilization in accordance with the European Communities Council Directive, the Norwegian Food Safety Authorities (FOTS permit #28918: Roles of the choroid plexus in brain physiology), and the animal experiment guidelines of Korea National Veterinary Research and Quarantine Service. The experimental procedures performed in the Republic of Korea were approved by the Korea University Institutional Animal Care & Use Committee (IACUC; KOREA-2019–0165) and were performed in accordance with the animal experiment guidelines of Korea National Veterinary Research and Quarantine Service. Embryonic, larval, juvenile and adult zebrafish were reared according to standard procedures of husbandry at 28.5°C.

For our experiments, the following zebrafish lines were used: *Gt(foxj1b:GFP)*,[23] *Tg(uas:NTR-mCherry)*,[77] *Tg(kdrl:GFP)*,[24] *Tg(elavl3:GcaMP6s)*,[70] *Gt(fabp7b:2A-Gal4vp16)*^{FRZCC1104} and *Tg(uas:starmaker-GFP)*^{nw22Tg}). Zebrafish were analyzed irrespective of their gender. Note that for zebrafish younger than 2–3 months, gender is not yet apparent. All zebrafish lines containing the *Gt(fabp7b:2A-Gal4vp16)*^{FRZCC1104} allele were maintained as heterozygous to avoid loss of fabp7b. Animals were either in the AB or pigmentless nacre^{b692} (*mitfa*$^{-/-}$)[71] background.

Generation of *Gt(fabp7b:2A-Gal4vp16)*^{FRZCC1104} knock-in zebrafish

To create the genetic line to label *fabp7b*-expressing cells specifically, the short homology mediated knock-in strategy was used.[72,73,78] First, a Cas9 target site was selected in exon 4 of *fabp7b* gene using by CHOPCHOP[76] (http://chopchop.cbu.uib.no/). The sgRNA was synthesized by the cloning-free gRNA *in vitro* synthesis[72,73] and Cas9 mRNA from the pT3TS-nCas9n plasmid (Addgene) with mMESSAGE mMACHINE T3 transcription kit (Thermo Fisher Scientific). To validate efficiency of the sgRNA, *fabp7b* sgRNA and Cas9 mRNA was microinjected into one-cell wildtype embryos and genomic DNAs were extracted from circa 20 injected embryos at 24 hpf. Then, T7 endonuclease I assay was performed.[74,79] Next, homology arms of the target vector were designed by the GtagHD (http://www.genesculpt.org/gtaghd/) and the pGTag-2A-Gal4vp16-B-actin plasmid (Addgene) was used as a donor vector.[72,73] The *fabp7b* targeting donor plasmid including 2A-Gal4vp16-B-actin was constructed and the plasmid was purified with the QIAGEN Plasmid Midi kit (QIAGEN) and PureYield Plasmid Miniprep System (Promega). 2 nL of a mixture of *fabp7b* sgRNA (50 pg), universal gRNA (25 pg), Cas9 mRNA (200 pg) and the target donor plasmid (10 pg) was injected into one-cell stage embryos of several UAS transgenic lines. The injected embryos expressing fluorescence in the choroid plexus (ChP) were screened and raised to adulthood (F0). To identify germline-transmitted lines, the F0 fish were crossed with several UAS transgenic lines and were validated based on ChP specific fluorescence in F1 embryos. Following selection of the germline-transmitting founder, we confirmed the integration of the 2A-Gal4vp16-B-actin DNA into the genome by PCR on the genomic DNAs of the fluorescence positive larvae. We verified that the 2A-Gal4vp16 DNA was integrated into the genomic area by performing PCR and sequencing at the 5′ and 3′ junctions of integration sites (Figure S6A).

Generation of *Tg(uas:starmaker-GFP)*^{nw22Tg} line

The open reading frame (ORF) of *starmaker* (*stm*: ENSDARG00000035694) was amplified by PCR from zebrafish cDNA. The amplified PCR products were fused to a C-terminal eGFP-Tag separated by a 5′-TCTAGAACTATA-3′ linker sequence containing an XbaI restriction enzyme site. The starmaker-GFP DNA was inserted into the pUAS-Self vector (gift from Sebastian Gerety) downstream of the zebrafish-optimized 5′-GCAAAC-3′ Kozak sequence through Gibson cloning. The starmaker sequence in this plasmid construct lacks the 45 base pairs corresponding to Exon 15 of the Ensembl transcript stm-202 (ENSDART00000105174.6), resulting in a 15 amino acid in-frame deletion.

To generate the transgenic line, 2 nL of a mixture of the uas:starmaker-GFP plasmid DNA (60 pg) and tol2 mRNA (10 pg) was microinjected into one-cell stage embryos. The injected embryos expressing red fluorescence in the eye lens were selected and raised to adulthood (F0). Germline-transmitting founders were identified by breeding with several Gal4 transgenic lines and selected based on RFP expression in the lens and predicted GFP signals in the Gal4 lines. Stable F1 embryos showing strong RFP signals were raised to adult zebrafish.

METHOD DETAILS

Immunohistochemistry and confocal microscope imaging

Zebrafish were euthanized by cold artificial fish water (AFW) or high dose MS222 in AFW. Larvae and juvenile were fixed in 4% paraformaldehyde (PFA), 1% DMSO and 0.3% Triton X-100 in PBS (phosphate buffered saline) (0.3% PBST) solution at 4°C overnight. The fixed samples were washed with 0.3% PBST three times and then the brains were dissected out. For adult, the brains were dissected out in cold artificial cerebrospinal fluid (aCSF) and then fixed with 4% PFA at 4°C overnight. The pineal gland was removed in samples used to image the forebrain ChP. For SV2 and ATP1A1 staining, the fixed samples were rinsed with PBST several times and they were dehydrated in 100% methanol (Sigma) and kept at −20°C overnight. They were rehydrated gradually through 75%, 50%, 25% methanol in 0.3% PBST solution steps for 5 min per each solution. Then they went into the permeabilization step described below. For Cldn5 antibody staining, the samples were fixed with Dent's fixative (80% Methanol/20% DMSO) at 4°C overnight. The fixed samples were rehydrated gradually through 75%, 50%, 25% methanol in 0.3% PBST solution steps for 5 min per each solution. They were washed with 0.3% PBST three times for 5 min and then they went into the blocking solution step, described below.

The samples were washed with 0.3% PBST three times for 30 min and then permeabilized by −20°C stored acetone for 10 min (larvae), 15 min (juvenile) and 1 h (adult) at room temperature (RT). Then the brains were washed again with 0.3% PBST three times for 30 min and immersed with blocking solution (0.1% bovine serum albumin (BSA) and 1% DMSO in 0.3% PBST) for over 2 h on shaker at RT. Samples were incubated in the blocking solution with anti-acetylated tubulin (1:500, Sigma-Aldrich), anti-4C4 (1:400, gift from Wittamer lab),[25] anti-Fabp7 (1:400, Sigma), anti-SV2 (1:100, Developmental Studies and Hybridoma Bank), anti-ATP1A1 (1:10, Developmental Studies and Hybridoma Bank) and anti-Cldn5 (1:100, Thermo Fisher Scientific) antibodies overnight at 4°C. On the next day, samples were washed with 0.3% PBST three times for 3 h and then immersed in the blocking solution for 2 h

on a shaker at RT. Subsequently, samples were incubated at 4°C overnight with secondary antibodies (goat anti-rabbit Alexa Fluor Plus 647 or goat anti-mouse Alexa Fluor Plus 647 (Thermo Fisher Scientific, 1:1000) and Alexa Fluor 488 tagged anti-GFP polyclonal antibody (Thermo Fisher Scientific, 1:500) to boost the GFP signals. On the third day, samples were incubated with 0.1% DAPI (Thermo Fisher Scientific) at RT for 30 min on shaker and then washed with 0.3% PBST three times for 3 h on shaker. Next, samples were transferred to the PBS solutions gradually increased glycerol concentrations (25%, 50% and 75% glycerol in PBS). After staining steps were finished, samples were imaged immediately or stored in 75% glycerol in PBS at 4°C before imaging. Samples were imaged using by a Zeiss LSM880 confocal microscope with an Examiner Z1 and a 20x Plan NA 0.8 objective.

Brain ventricle injection and confocal microscope imaging

To visualize the brain ventricles and CSF, we followed our previous protocols.[21,52] Adult zebrafish were first euthanized by cold AFW. The adult brains were then dissected in cold aCSF and mounted on sylgard using a metal pin.[52,80,81] The injection mixture containing 70 kDa rhodamine B isothiocyanate-dextran (RITC-dextran; Sigma-Aldrich) dissolved in aCSF at a final concentration of 10 mg/mL. The injection needles were pulled with a Sutter Instrument Co. Model P-2000, from thin-walled glass capillaries (1.00 mm; WPI). The needle tip was opened by cutting with fine forceps. A microinjector (Eppendorf Femtojet 4i) was used to microinject around 15 nL of the mixture solution into the telencephalic ventricle. After injection, the adult brain explants were instantly transferred to the confocal microscope and imaged with a 20x water-immersion objective (Zeiss, NA 1.0, Plan-Apochromat) at RT. The laser power was adjusted according to the depth of imaging.

Hybridization chain reaction (HCR) and confocal microscope imaging

HCR was performed as described hereafter based on our prior method.[82] Zebrafish were euthanized by cold AFW. Juvenile were fixed in in 1 mL of 4% PFA in DPBS (1 X Dulbecco's phosphate-buffered saline) at 4°C overnight. Then, the fixed samples were washed with 0.1% Tween 20 in DPBS (DPBST) three times for 5 min and then the brains were dissected out. For adult, the brains were dissected out in cold aCSF and then fixed with 4% PFA in DPBS at 4°C overnight. The pineal gland was removed in samples used to image the forebrain ChP. Then, the fixed adult brains were washed 3 × 5 min with DPBS. The samples were directly transferred to methanol for overnight incubation at −20°C. The next day, the samples were rehydrated with 75%, 50%, 25% methanol in DPBST steps for 5 min (75%, 50% and 25% methanol in DPBS), and then washed for 5 min with DPBST. The brains were then treated with proteinase K (30 μg/mL) for 45 min at RT. After the treatment, they were rinsed with two washes of DPBST without incubation. After then, they were fixed with 4% PFA in DPBST for 20 min at RT. The brains were then washed 5 × 5 min with DPBST.

Around 3–4 juvenile brains or single adult brain were transferred to a 1.5 mL tube, respectively. The samples were then pre-hybridized with 500 μL of hybridization buffer for 30 min at 37°C. The HCR probes were prepared by adding 2 pmol of each probe set to 500 μL of hybridization buffer at 37°C. The pre-hybridization solution was removed, and the probe solution was added to the tubes and incubated at 37°C overnight. The next day the samples were washed 4 × 15 min with 500 μL of wash buffer at 37°C. The samples were then washed 2 × 5 min with 5 x SSCT at RT.

The samples were then treated with 500 μL of amplification buffer for 30 min at RT. The amplifiers were prepared separately by using 30 pmol of hairpin h1 and 30 pmol of hairpin h2 by snap cooling 10 μL of 3 μM stock (heat at 95°C for 90 s and cool to RT in a dark drawer for 30 min). The HCR hairpin solution was prepared by adding snap-cooled h1 hairpins and snap-cooled h2 hairpins to 500 μL of amplification buffer at room temperature. The pre-amplification solution was removed, and the samples were incubated with hairpin solution overnight in the dark at RT. The next day, the samples were washed with 500 μL of 5 x SSCT at RT for 2 × 5 min, 2 × 30 min and 1 × 5 min, respectively. The samples were then washed 1 × 5 min with DPBST and incubated with 0.1% DAPI (Thermo Fisher Scientific) in DPBST at RT for 30 min. They were washed 3 × 5 min with DPBST and then they were treated with a series of glycerol in DPBS (25, 50 and 75% glycerol with DPBS). After the staining, the samples were stored in 75% glycerol in DPBS at 4°C or imaged immediately. The samples were images using a Zeiss Examiner Z1 confocal microscope with a 20x plan NA 0.8 objective.

Transmission electron microscopy

Sample fixation, staining and embedding

Dissected adult brains were trimmed nearby the forebrain ChP by a razor blade in cold aCSF, and fixed with 2.5% glutaraldehyde and 4% PFA in 0.15 M cacodylate (pH 7.4) overnight at RT. For the dissection, the pineal gland was not removed and the dissected brains were trimmed into smaller pieces. For the juvenile fish, only jaw and trunk were removed in cold aCSF after cold AFW euthanasia. Then, the juvenile samples were fixed with the identical fixative overnight at RT. Next, the trimmed brains were encapsulated with 4% ultra-low melting agarose in 0.1M PB (phosphate buffer) and the access of agarose around the trimmed brain were removed with a razor blade. The samples were put in 2.5% glutaraldehyde in 0.15 M cacodylate (pH 7.4) and storage at 4°C. For preparation and *en bloc* staining a microwave (Pelco Biowave Pro+) was used with an established protocol with minor modifications[83,84](Table S1). The procedure includes successive exposures of the sample to 2% OsO4 in 0.15 M cacodylate buffer, 2.5% potassium ferrocyanide in 0.15 M cacodylate buffer, filtered 320 mM pyrogallol in aqueous solution (pH 4.1), 1% OsO4 in aqueous solution, filtered 320 mM pyrogallol in aqueous solution (pH 4.1), 1% OsO4 in aqueous solution, filtered 1% uranyl acetate in aqueous solution and filtered lead aspartate solution (0.02 M lead nitrate and 0.03 M aspartic acid, pH 5.5). Double rinses in pure filtered water were performed between the staining steps.

Samples were then dehydrated through a graded ethanol series (20%, 50%, 70%, 90%, 100%, 100%) and then into pure acetone (2 × 100%). After acetone, samples were infiltrated and incubated in 812 Epon resin diluted with ethanol (25%, 50%, 75%, 100%). In the end samples were placed in embedding molds with pure resin and cured at 60°C for 75 h.

Sample sectioning

Embedded samples were trimmed using an ultramicrotome (Leica EM UC7) with a dry glass knife. Sections of 1 μm were cut, put on a microscope slide and stained with toluidine blue for orientation with light transmission microscopy. The area of interest was then selected for ultrathin sectioning. Ultrathin sections (60 nm) were cut with an ultramicrotomy (Leica EM UC7) using a diamond knife (Diatome), and subsequently collected on slot Copper grid with Formvar support film.

Microscopy

The grids were viewed with a TEM (JSM-1011, JEOL) operating at 80 kV. Images were captured with a Morada digital camera with Radius software version 2.0 (EMSIS GmbH).

Total RNA sequencing and transcriptomic analysis

Total RNA preparation and RNA sequencing

To extract total RNA from the forebrain ChP, adult zebrafish (Nacre and AB, 6 - 8-month-old, >3 cm) were euthanized by cold AFW and the brains were dissected out in cold aCSF. The forebrain ChPs were collected after removing the pineal gland. The dissected forebrain ChPs were kept temporarily in 1.5 mL tubes containing 20 μL RNAlater (Thermo Fisher Scientific) on ice until RNA extraction steps started. Two batches of samples were prepared, and each batch had from 12 to 19 forebrain ChPs. To lyse the forebrain ChPs, TRIzol solution (500 μL, Thermo Fisher Scientific) was added and the tissues were homogenized through 27-gauge needles 15–18 times. More TRIzol (500 μL) was added into the tubes and the dissociated tissues were incubated for 5 min at RT. Chloroform (Sigma-Aldrich, 200 μL) was added to the samples and the tubes were inverted for several times to mix them. These were kept for 2 min at RT and centrifuged at 4°C for 15 min at 12,000 rpm. Then colorless supernatants including total RNAs were purified by two different methods using glycogen, or spin columns.

For the glycogen method, the RNA supernatant was transferred to a new tube and 0.5 μL glycogen solution (20 mg/mL, final glycogen mass: 10 μg) was added. Then, isopropanol (500 μL) was added to the sample, mixed by inverting and incubated on ice for 10 min. Then, the sample was centrifuged for 15 min at 12,000 rpm at 4°C. The supernatant was discarded, and the pellet was washed with 1 mL 70% ethanol (w/nuclease-free water) chilled at −20°C. The pellet was air-dried on ice for 2–5 min and dissolved in 70 μL nuclease-free water (Invitrogen). The sample was then treated with 10 μL DNase enzyme (QIAGEN) for 10 min at RT to remove DNA in the RNA samples. To isolate the RNAs, phenol-chloroform ethanol precipitation was performed. The DNase treated RNA sample was added to phenol-chloroform (pH8.0, 100 μL) and mixed for 5–10 s by inverting. The RNA was centrifuged for 8 min at 12,000 rpm at 4°C. The clear supernatant was transferred to a new tube, treated with chloroform (100 μL) and mixed for 5–10 s by inverting. Following centrifugation at 12,000 rpm for 8 min at 4°C, the supernatant was precipitated with 10 μL 4M Ammonium Acetate buffer (100 μL) and 100% ethanol 330 μL for 30 min at −20°C and centrifuged at 12,000 rpm for 30 min at 4°C. The pellet was washed with 70% EtOH (w/nuclease-free water, 500 μL) and air dried on ice for 2–5 min. The pellet of RNAs was dissolved in 20 μL nuclease-free water (Thermo Fisher Scientific).

For the spin column method, the RNA supernatant was mixed to identical amount of isopropanol, loaded on RNA grade spin columns (QIAGEN, RNeasy Mini kit) and centrifuged for 30 s at 8,000 rpm. The spin columns were washed with 700 μL Buffer RW1 and 350 μL Buffer RW1 followed by DNase enzyme treatment in Buffer RDD for 10 min (10μL DNase in 70 μL Buffer RDD per column) at RT. After treatment, the column was washed with 350 μL Buffer RW1 and 500μL Buffer RPE. To elute the RNAs from the columns, 20 μL nuclease-free water was added and incubated for 2 min. The RNAs were centrifuged for 1 min at 8000 rpm and collected in tubes. The concentrations of four eluted RNAs were quantified using Nanodrop (Thermo Fisher Scientific) and stored at −80°C before RNA sequencing.

The quality of RNA samples was analyzed by bioanalyzer at Novogene. Due to low amount of quantity in the RNA samples, the RNAs were pre-amplified using by the SMARTer kit and RNA sequencing (paired-end 150 bp, with 12 Gb output) was performed on an Illumina NovaSeq 6000 (Illumina) at Novogene.

Transcriptomic analysis

RNA sequencing data for human, rat, and mouse were obtained from the GEO repository.[85,86] Rat ChP transcriptome data was obtained with GEO accession number GSE194236 (sample: SRR17713531).[36] The human ChP transcriptome data was obtained with GEO accession number GSE137619 (samples: SRR10134643-SRR10134648).[34] The mouse ChP transcriptome data was obtained from GEO accession number GSE157386 (samples; SRR12576642-SRR12576645, SRR12576650-SRR12576653).[35] The zebrafish ChP transcriptome data was obtained from this study.

All program parameter settings for library building and mapping, together with all scripts for the gene annotation and analysis are available at https://github.com/Sorennorge/Choroid-plexus-orthology-study and https://doi.org/10.5281/zenodo.11230620. The sequencing data for human and mouse were quality controlled with fastqc,[87] and the human data were trimmed with Trimmomatic[88] (Sliding window 4:20, minimum length of 35 bp). The obtained sequencing data were mapped to reference genome for human (Homo sapiens GRCh38 v.104), rat (Rattus norvegicus Rnor_6.0 v.104), mouse (Mus musculus GRCm39 v.104), and zebrafish (Danio rerio GRCz11 v.104) using Spliced Transcripts Alignment to a Reference (STAR) RNA-seq aligner (v. 2.7.2a).[89] The reference genomes were trimmed prior to mapping to only contain gene/transcripts of biotype 'protein coding'. The mapped alignment by STAR was

normalized to TPM with RSEM (RNA-Seq by Expectation Maximization v. 1.3.3).[90] The means of calculated TPM were used for the further analysis of human, mouse, and zebrafish. Especially, the TPMs of zebrafish presented in Table S2 are averaged counts from the 2 sequencing datasets. Gene information for 'gene symbol' (gene names) and orthologs were gathered from Ensembl biomart.[91,92] The duplicated genes in zebrafish were counted as separate genes. For Figures 2C and S5F, the expression levels of duplicated genes were summed into one TPM value: if there were two zebrafish duplicated genes but only one human gene, TPMs were added from the two duplicated zebrafish genes to compare with the TPM of the one human gene. The density analysis was generated utilizing the seaborn distribution python library.[93,94] The Venn diagrams were generated utilizing nVennR package for R.[95] Transporters were collected based on the protein class which was obtained by utilizing the Panther database[96] with gene symbols. Transporters were ranked based on TPM amongst transporters within each species. Hereafter, the transporter table were sorted based on the mean rank for all four species. To compare orthologous transporters, all the genes that have orthologous genes in the other species were collected. The non-orthologous genes, which are not annotated as having orthologues in the other species were excluded from further analysis.

Cloning zebrafish *fabp7b* and whole mount RNA *in situ* hybridization

To isolate *fabp7b* gene, primers were designed to clone *fabp7b* ORF from Ensembl (*fabp7b*: ENSDARG00000034650). *Fabp7b* ORF was amplified from 3 dpf cDNA using the designed primers by PCR and cloned into pGEM-T easy vectors (Promega). To synthesize fabp7b RNA probe, the cloned vector was linearized by SacII restriction enzymes (New England Biolabs) at 37°C for 1 h in 30 μL solution (3 μL CutSmart buffer, 2 μL SacII enzyme and 25 μL fapb7b ORF cloned vectors) and then purified by the ethanol precipitation described in the section of total RNA preparation above. The linearized purified vectors were transcribed using the SP6 RNA polymerase and DIG-oxygenin labeling mixture (Roche) for 1 h at 37°C in 20 μL mixture (2 μL 10x transcription buffer, 2 μL 10x DIG RNA labeling mix, 1 μL RNase inhibitor, 2 μL SP6 polymerase, and 13 μL linearized plasmid. The synthesized RNA probe was treated with 2 μL Dnase for 10 min at 37°C to remove left DNA plasmid. Then the probe was purified by ethanol precipitation and dissolved in 20 μL formamide and stored at −20°C. The RNA probe integrity was confirmed by gel electrophoresis and the probe quantity was measured by NanoDrop (Thermo Scientific).

To prepare samples for whole mount RNA *in situ* hybridization, 7 dpf zebrafish larvae were euthanized by MS222 (Sigma-Aldrich) in E3 medium until movements ended and fixed with 4% paraformaldehyde (PFA) in 0.2% PBST (PBS with 0.2% Triton X-100) overnight at 4°C. The fixed larvae were rinsed with PBST several times and the brains were dissected out from the larvae with fine forceps. The larval brains were dehydrated in 100% methanol (Sigma) and kept at −20°C.

RNA *in situ* hybridization was performed by alkaline phosphatase-NBT/BCIP (Roche) chromogenic reaction, as described earlier.[79,97] The brains were rehydrated gradually through 75%, 50%, 25% methanol in 0.2% PBST solution steps for 5 min per each solution. Following 3 washes for 15 min in 0.2% PBST, the samples were digested with proteinase K (10 μg/mL) for 10–20 s, fixed in 4% PFA solution for 20 min at RT and then washed by 0.2% PBST. The samples were prehybridized at 65°C for 3 h in hybridization buffer (50% formamide (Junsei), 5X SSC (Sigma-Aldrich), 50 μg/mL heparin, 500 μg/mL tRNA, 0.2% Triton X-100), followed by hybridization at 60°C overnight with 200 ng RNA probe/200 μL hybridization buffer. The samples were subsequently washed twice for 20 min in 50% formamide/2X SSCT, twice for 15 min in 2X SSCT, three times for 20 min in 0.2X SSCT and 0.1XSSCT once for 10 min at 65°C. Following three washes in 0.1% PBT (0.1% tween 20 in PBS) at RT on shaker, the samples were blocked in blocking solution (5% sheep serum, 2 mg/mL BSA) for 2 h at RT on shaker and incubated overnight at 4°C in AP-*anti*-DIG antibody (Roche) diluted 1:4000 in blocking solution. The next day, the samples were washed 10 ×15 min in 0.1% PBT, followed by 3 × 5 min in staining buffer (100 mM Tris, pH 9, 50 mM MgCl2, 100mM NaCl, 0.1% Tween 20) at RT. The samples were stained for 4–12 h in NBT/BCIP solution (1:50 dilution of NBT/BCIP (Roche) in staining buffer). The staining was terminated by several washes with 0.1% PBT at RT and fixation with 4% PFA solution overnight at 4°C. The samples were washed with 0.1% PBT several times at RT and transferred to 75% glycerol in PBS. The brains were imaged in the bright field mode of Ni-U fluorescent microscope (Nikon) with DS-Ri2 camera.

Metronidazole treatment

To ablate the epithelial cells in the ChP, juvenile *Gt(fabp7b:2A-Gal4vp16);Tg(uas:NTR-mCherry);Gt(foxj1b:GFP)* zebrafish and their mCherry negative *Gt(foxj1b:GFP)* siblings were used. 30 larvae from each line were kept in a nursery tank (Techniplast) before metronidazole (MTZ) treatment to produce similar size of the juvenile fish. At 14 dpf, *Gt(fabp7b:2A-Gal4vp16);Tg(uas:NTR-mCherry);Gt(foxj1b:GFP)* and mCherry negative *Gt(foxj1b:GFP)* fish were treated with either 10 mM MTZ (Sigma-Aldrich) in 0.2% DMSO in AFW for 24 h (from 14 to 15 dpf). As another control group, *Gt(fabp7b:2A-Gal4vp16);Tg(uas:NTR-mCherry);Gt(foxj1b:GFP)* fish were also treated with 0.2% DMSO in AFW for 24 h.[77,98] Three fish were placed in a Petri dish containing 50 mL of 10 mM MTZ/0.2% DMSO in AFW or 0.2% DMSO in AFW in a 28°C incubator, with regular light/dark cycles (14 h light/10 h dark). Following treatment, the fish were washed with fresh AFW three times and transferred to the nursery tank until the start of the experiments. MTZ treatment experiments were performed on three different batch of fish on different dates. Data were collected and analyzed from the three experiments. The 0.2% DMSO and 10 mM MTZ treated *Gt(fabp7b:2A-Gal4vp16);Tg(uas:NTR-mCherry);Gt(foxj1b:GFP)* fish were only used for transmission electron microscopy and the samples were collected from two different batch of fish on an identical date.

Intravenous injection and wholemount zebrafish *in vivo* live imaging

For intravenous injection, juvenile fish (17–18 dpf) were anesthetized in MS222 diluted in AFW and mounted in 1.5% low melting agarose with the trunk veins facing upwards. The body size of each fish was measured with a ruler. 10 kDa dextran Alexa Fluor 647 (Thermo Fisher Scientific) was dissolved in PBS at a final concentration of 10 mg/mL.[99] Intravenous injections were performed as described above for the ventricular injections: injection needles were pulled with the identical method and the needle tip was opened by cutting with forceps. A microinjector (Eppendorf Femtojet 4i) was used to microinject circa 2–3 nL of the fluorescent dye into the cardinal vein near the tail. Following injection, the fish were released from agarose and placed in MS222 diluted AFW for 1 h. Then, the fish were remounted in 1.5% low melting agarose with the dorsal brain facing upwards to image the tel- or rhombencephalon areas including forebrain and hindbrain ChP. For Figures S8 and S10 kDa dextran Alexa Fluor 647 (Thermo Fisher Scientific), 3 kDa dextran TMR (Thermo Fisher Scientific) and 70 kDa dextran FITC (Sigma) were dissolved in PBS at a final concentration of 10 mg/mL per each dye. Intravenous injections of the dye mixtures were performed as described above and each brain ventricle was imaged at various time points: 30, 60, 90 and 120 min. One injected fish was used for only one timepoint. The fish were transferred to the confocal microscope and Z-stacks images were obtained with 2.5 μm z-steps by a 20x water-immersion objective (Zeiss, NA 1.0, Plan-Apochromat) at RT.

Whole body images of zebrafish juveniles

Juvenile fish (17dpf) used in the ablation experiments were anesthetized in MS222 diluted in AFW and mounted in 1.5% low melting agarose laterally. The mounted fish were imaged under a stereomicroscope (Olympus) with the camera of a mobile phone. For scaling, the fish were imaged with a ruler.

Imaging processing

Confocal stacks were stitched in Fiji/ImageJ[75] using the pairwise stitching plugin[100] for images shown in Figures 3E1, S6B, S6D1, and S7B1. All fluorescence images except the stitched images were deconvoluted in the Huygen software (Scientific Volume Imaging) using the standard Deconvolution Express function. Raw images were used for all analysis and quantifications.

QUANTIFICATION AND STATISTICAL ANALYSIS

All quantifications were performed using by ImageJ/Fiji. Plots and statistical analyses were generated using MATLAB. The statistical tests used and description of the numbers of observations are indicated in each figure legend.

Quantification of 4C4 positive cell numbers of in the tela choroidea, choroid plexus

The 4C4 expressing cells at the apical and basal sides of the epithelial cells were counted on confocal stacks within a specific volume (width x length x height (μm): 400 x 400 x (125–200) in the tela choroidea and forebrain ChP. 400 x 400 x (250–300) in the hindbrain ChP. The heights were variable due to the angles of imaging and size of the target brain regions. For the cell numbers in the juvenile brain, all the cells in each area were counted. The numbers were imported and plotted in MATLAB.

Quantification of NTR-mCherry expression in the tela choroidea, choroid plexus and subcommissural organ

To measure the percentage of NTR-mCherry-expressing areas in each area, the confocal stacks from the DMSO treated control *Gt(fabp7b:2A-Gal4vp16);Tg(uas:NTR-mCherry);Gt(foxj1b:GFP)* fish at 17–18 dpf (n = 10) were utilized. First, max projection images of the confocal stacks were generated by ImageJ/Fiji which contained GFP-expressing the tela choroidea, forebrain, hindbrain ChPs and subcommissural organ (SCO). Then, the region of interest (ROI) in GFP and mCherry-expressing area was drawn manually for each fish and recorded. The size of the mCherry-expressing area was normalized to the GFP-expressing area for each fish. The values were converted to percentages. All datapoints were imported and plotted in MATLAB.

To quantify the ablation efficiency in the tela choroidea, forebrain, hindbrain ChPs and SCO, max projection images of the confocal stacks were generated from control and ablation groups. A ROI comprising the GFP-positive area was drawn for each fish. The GFP-positive area was normalized by the average value of all GFP-positive area obtained from controls (DMSO and Ctrl MTZ treated groups). All values were imported and plotted in MATLAB.

Quantification of the size of brain ventricles on confocal images

We quantified the size of the anterior telencephalic ventricle (ant. TV) on images showing a dorsal view, and the posterior telencephalic/anterior di-/mesencephalic ventricle (post. TV & D/MV) and rhombencephalic ventricle (RV) on resliced images showing the sagittal view. We selected these view angles as they allowed us to distinguish the brain ventricles from blood plasma and skin.

For measuring the ant. TV areas, 12.5 μm thick (6 slices) maximum intensity projections of confocal stacks were used. For the rest of the ventricular areas, images of the confocal stacks were resliced by ImageJ/Fiji to visualize the sagittal view of the brain. Then 10 μm thick (5 slices) maximum intensity projection of the stacks were utilized. ROIs were drawn on the far-red channel showing Alexa 647 positive ventricles. The values were imported and plotted in MATLAB.

Quantification of the fluorescent intensities on confocal images

To quantify the fluorescent intensities in the blood, ventricle, and parenchyma, we used the same sections and areas of the brain where the ventricular size was measured. Mean fluorescent intensities were measured by ImageJ from ROIs drawn on blood vessels, parenchyma and ventricle for each section and each area. The fish shown the collapsed ventricles were excluded. As a result, for each fish, 6 or 5 fluorescent intensities were collected per area. Intensities were normalized to the size of the ROI and averaged to obtain the "mean intensities per area". The values in the parenchyma ($Intensity_{parenchyma}$) and ventricle ($Intensity_{ventricle}$) were further normalized by the values in the blood ($Intensity_{blood}$). All datapoints were collected and imported to MATLAB.

Quantification of the brain parenchyma and fish size on confocal images

To check the size of brain parenchyma in the control and ablated groups, the width of telencephalon and rhombencephalon was measured by ImageJ/Fiji. The tel-/rhombencephalic width corresponds to the widest area of the tel-/rhombencephalon, where no ventricles are observed to avoid a potential impact of the ventricles on the measurements. The rhombencephalon, parenchyma width was measured where the RV was widest. The values were imported and plotted in MATLAB. The fish size was measured using a ruler before intravenous injection and these datapoints were also imported and plotted to MATLAB.